PhD in Molecular Medicine
XXXII Cycle

miR-139-5p-PI3K/AKT/mTORC1 network has a role in supratentorial pediatric Low Grade Gliomas (pLGGs)

Candidata: Martina Chiacchiarini Matr. 1318814

Relatore: Prof.ssa Elisabetta Ferretti

Summary

1. Abstract

Aim: Pediatric low-grade gliomas (pLGGs) are a heterogeneous group of brain tumours associated with a high overall survival: however, they are prone to recur and supratentorial lesions are difficult to resect, being associated with high percentage of disease recurrence. Our aim was to shed light on the biology of pLGGs.

Methods: We performed microRNA profiling on 45 fresh-frozen grade I tumour samples of various histological classes, resected from patients aged ≤16 years. We identified 93 microRNAs specifically dysregulated in tumours as compared to non-neoplastic brain tissue. Enriched pathway analysis of the microRNAs signature revealed PI3K/AKT signaling as the first enriched oncogenic signaling. Although, activation of the PI3K/AKT pathway has been previously reported in these tumours, the activation mechanisms that are involved have not been investigated yet.

Results: Among significantly down-regulated microRNAs in supratentorial pLGGs cohort the miR-139-5p was of interest since its targets include the gene encoding the PI3K's (phosphatidylinositol 3-kinase) catalytic unit, PIK3CA. Thus, the role of miR-139-5p in regulating PI3K/AKT signaling has been investigated by the use of primary patients derived cells. In these models the overexpression of miR-139-5p inhibited pLGG cell proliferation and decreased the phosphorylation of PI3K target AKT and phosphorylated-p70 S6 kinase (p-p70 S6K), a hallmark of PI3K/AKT/mTORC1 signaling activation. The effect of miR-139-5p was mediated by PI3K inhibition, as suggested by the decrease in proliferation and phosphorylation of AKT and p70 S6K after treatment with the direct PI3K inhibitor LY294002.

Conclusions: These findings provide the first evidence that down-regulation of miR-139-5p in supratentorial pLGG drives cell proliferation by derepressing PI3K/AKT signaling.

2. Introduction

2.1 Pediatric low-grade gliomas

The most commonly diagnosed brain tumours in children are low-grade gliomas (LGGs), representing over 30% of tumours affecting the Central Nervous System (CNS) (Packer R.J. et al., 2016). Pediatric LGGs (pLGGs) include different entities, as defined by the recently revised World Health Organization (WHO) Classification of Central Nervous System (CNS) Tumours, which is based on both histological and molecular features (Louis D.N. et al., 2016). This classification identifies nine categories of CNS tumours, of which four include tumours of glial or glioneuronal origin:

- Diffuse astrocytic and oligodendroglial tumours

- Other astrocytic tumours

- Other gliomas

- Glioneuronal tumours

Furthermore, the WHO classification system categorizes these tumours starting from grade I (lowest grade) to grade IV (highest grade), based upon histopathologic characteristics such as:

• similarity with normal cells (atypia);

• growth rate (mitotic index);

• growth rate and death of tumour cells in the neoplastic focus (necrosis);

• potential diffusion rate (widespread or focal);

• blood flow (vascularization)

Low-grade gliomas (LGGs) consist of grade I tumours, which contain none of the mentioned histologic features, and grade II tumours, characterized by the presence of cytologic atypia alone (Louis D.N. et al., 2016), and are classified in:

Table 1. Classification of diffuse gliomas.

Diffuse gliomas	**WHO grade**	**Histological features (Pathological Anatomy)**	**Localization (Clinical Diagnosis)**
Diffuse Astrocytoma (DA)	II	Irregular nucleus and hyperchromia; low mitotic index and absence of vascular proliferation.	Brain hemispheres. In pediatric age it can also arise in the brain stem or in the spinal cord.
Oligodendroglioma (OG)	II	Regular and uniform nucleus, clear cytoplasm, with a definite aspect to "honeycomb".	Bark and white matter of the brain hemispheres.
Oligoastrocytoma (OA)	II	Mixed characteristics between the two cell types.	Brain hemispheres.

Table 2. Classification of astrocytic tumours.

Astrocytic tumours	**WHO grade**	**Histological features (Pathological Anatomy)**	**Localization (Clinical Diagnosis)**

Pilocytic astrocytoma (PA)	I	Biphasic architecture with compact areas and non-homogeneous areas. The former show "piloid" processes and often multiple Rosenthal fibers. The latter show eosinophilic granular bodies. Limited mitoses.	Generally in the cerebellum, optical pathways, III ventricle. Sometimes basal ganglia or cerebral hemispheres.
Astrocytoma Pilomixoid (PMA)	II	Fusiform cells associated with perivascular dispositions on a loose fibrillar and myxoid background lacking Rosenthal fibers.	At the level of the chiasmus.
Gigantocellular Subependimal Astrocytoma (SEGA)	I	High phenotypic variability, hyalinization of the blood vessel wall, lymphocyte infiltrates and calcification. Furthermore, mitotic activity can be observed.	It originates in the wall of the lateral ventricles, near the foramen of Monro.
Pleomorphic Xanthoastrocytoma (PXA)	II	Large, pleomorphic tumour cells; often they have many eosinophilic and aggregated granular bodies of lymphocytes.	Predominantly in the cerebral hemispheres.

Table 3. Classification of other gliomas.

Other gliomas	**WHO grade**	**Histological features (Pathological Anatomy)**	**Localization (Clinical Diagnosis)**
Angiocentric glioma (AG)	I	Tumour characterized by monomorphic, bipolar or less frequently epithelial cells with parallel or radial orientation to the vessel walls.	Brain hemispheres.
Astroblastoma	I	Tumour cells with large cytoplasm, radially oriented around blood vessels with extensive processes.	Brain hemispheres.

Table 4. Classification of glioneuronal tumours**.**

Glioneuronal tumour	**WHO grade**	**Histological features (Pathological Anatomy)**	**Localization (Clinical Diagnosis)**

Ganglioglioma (GG)	I	Cancer ganglion cells generally have dysmorphic features and abnormal orientation. They often have granular eosinophilic bodies.	Temporal lobe.
Ganglioglioma/ Astrocytoma infantile desmoplastic (DIG/DIA)	I	Characterized by the presence of a desmoplastic stroma rich in reticulina	Brain hemispheres
Disembrioplastic Neuroepithelial Tumour (DNET)	I	Specific glioneuronal component, represented by axonal extensions surrounded by oligodendrocytes immersed in patches of loose substance in which the neuronal bodies seem to "float".	The temporal lobe, the floor of the III ventricle and the hypothalamus.

The vast majority of pLGGs are pilocytic astrocytomas (PAs, Figure 1), and they are therefore the ones that have been studied most thoroughly.

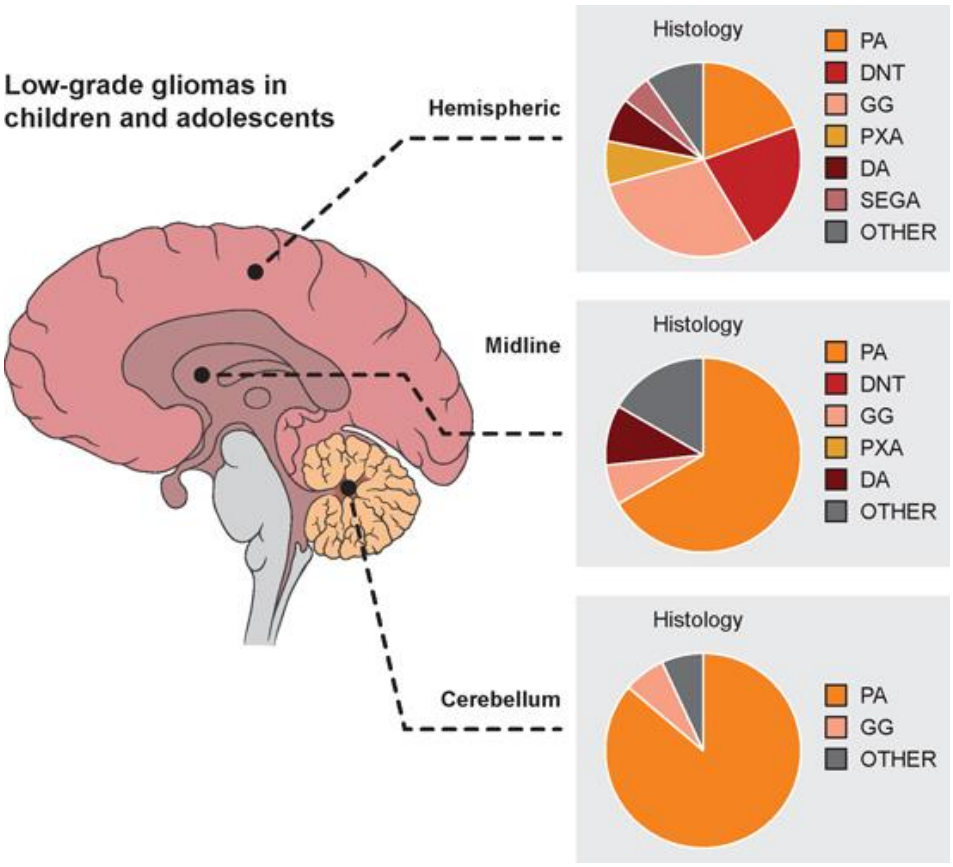

Figure 1. Distribution of histological subtypes of CNS tumours between adolescents and children. (Filbin M.G. et al., 2018)

These tumours are driven by dysregulated signaling through the MAPK/ERK pathway, which leads to growth arrest referred to as oncogene-induced senescence (OIS) (Pfister S. et al., 2009; Packer R.J. et al., 2016). Less is known about the biological characteristics of less common pLGGs which include, among others, gangliogliomas (GGs), disembryoplastic neuroepithelial tumours (DNETs), and angiocentric gliomas (AGs). The location of pLGGs also has a major impact on the patients' outcome since it determines the tumour's resectability. Infratentorial pLGGs, which occur mainly in the cerebellum, can often be cured by surgery. Supratentorial tumours and those arising in the brainstem are much more difficult to resect, and residual or recurrent disease is, therefore, a common event. The latter are treated with radiotherapy or conventional chemotherapy (e.g. SIOP-LGG 2004 protocol). However, both treatments are associated with substantial long-term toxicity, and these tumours frequently evolve into chronic disease with high morbidity (Pfister S. et al., 2009; Packer R.J. et al., 2016; Zhang J. et al., 2013; Garcia M.A. et al., 2016; Sturm D. et al., 2017).

The genomic landscape of pLGGs is now being defined. The most frequent genetic alterations are the KIAA1549-BRAF fusion gene and the BRAF V600E single point mutation (Zhang J. et al., 2013). The BRAF gene is located on the long arm of chromosome 7q34 and encodes a protein involved in the MAPK signaling pathway, which is a conserved signaling cascade, which utilizes a series of protein kinases to transduce signals from the cell membrane to the nucleus, Figure 2. It plays a crucial role in mediating a range of biological functions, including cell growth, survival, and differentiation.

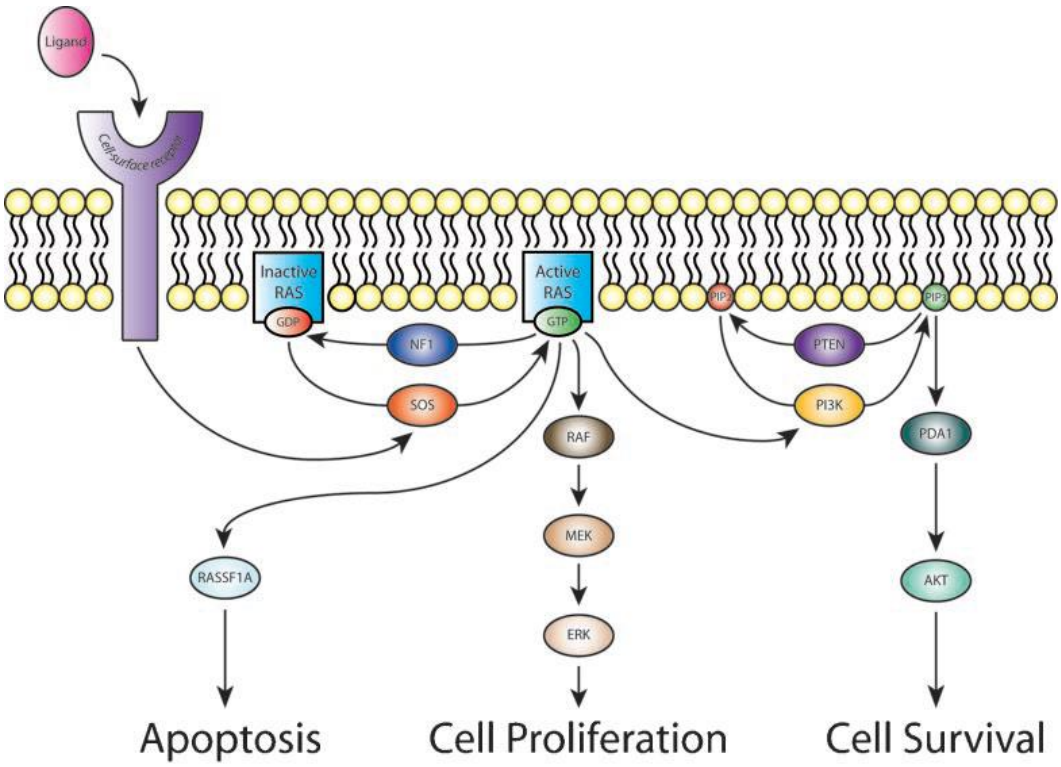

Figure 2. Schematic representation of the MAPK pathway. The initiating event in MAPK pathway activation occurs when an extracellular ligand binds to one of several cell–surface receptors. The receptor-ligand complex activates an intracellular signaling cascade with the binding of RAS to GTP and its consequent activation. This process can be reversed by some GTPases, such as Neurofibromine 1 (NF-1), which catalyze the conversion of the active RAS-GTP form to the inactive RAS-GDP form. When RAS is activated it can interact with more than 20 different substrates, including members of the RAF family and PI3K (Schubbert S. et al., 2007). This interaction allows the three RAF kinases (ARAF, BRAF and RAF1) to phosphorylate MEK1 and consequently activate ERK1 and ERK2. ERK proteins can phosphorylate different effector molecules with induction of cell proliferation (Schubbert S. et al., 2007). PI3K instead catalyzes the transformation of the phosphorylation of phosphatidylinositol-4,5-bisphosphate (PIP2) and the subsequent production of phosphatidylinositol-3,4,5-trisfosfate (PIP3), a process inhibited by phosphatase homolog of the phosphatase and tensin (PTEN). The accumulation of PIP3 promotes the

recruitment of PDK1 at the membrane level, where it phosphorylates AKT, which in turn can phosphorylate a series of proteins that favor cell survival (Tatevossian R.G. et al., 2010).

The MAPK/Erk signaling cascade is activated by a wide variety of receptors involved in growth and differentiation including receptor tyrosine kinases (RTKs), integrins, and ion channels. The specific components of the cascade vary greatly among different stimuli, but the architecture of the pathway usually includes a set of adaptors (Shc, GRB2, Crk, etc.) linking the receptor to a guanine nucleotide exchange factor (SOS, C3G, etc.) transducing the signal to small GTP-binding proteins (Ras, Rap1), which in turn activate the core unit of the cascade composed of a MAPKKK (Raf), a MAPKK (MEK1/2), and MAPK (Erk). An activated Erk dimer can regulate targets in the cytosol and also translocate to the nucleus where it phosphorylates a variety of transcription factors regulating gene expression (Schubbert S. et al., 2007). Activated RAS is also capable of interacting with members of the phosphatidylinositol 3-kinase (PI3K) family. In particular, PI3K catalyzes the accumulation of PIP3, which promotes the recruitment of PDK1 at the membrane level, where it phosphorylates AKT, which in turn can phosphorylate a series of proteins that favor cell survival (Tatevossian R.G. et al., 2010). One of the main mediators downstream of the PI3K/AKT pathway is the mammalian target of rapamycin (mTOR), in the form of 2 complexes: mTORC1 and mTORC2, as shown in Figure 3. Following its activation, the mTORC1 complex induces an increase in protein synthesis, stimulates cell growth and survival. The mTORC2 complex is less known, but appears to regulate metabolism, survival through AKT activation and cytoskeletal organization (Hütt-Cabezas M. et al., 2013).

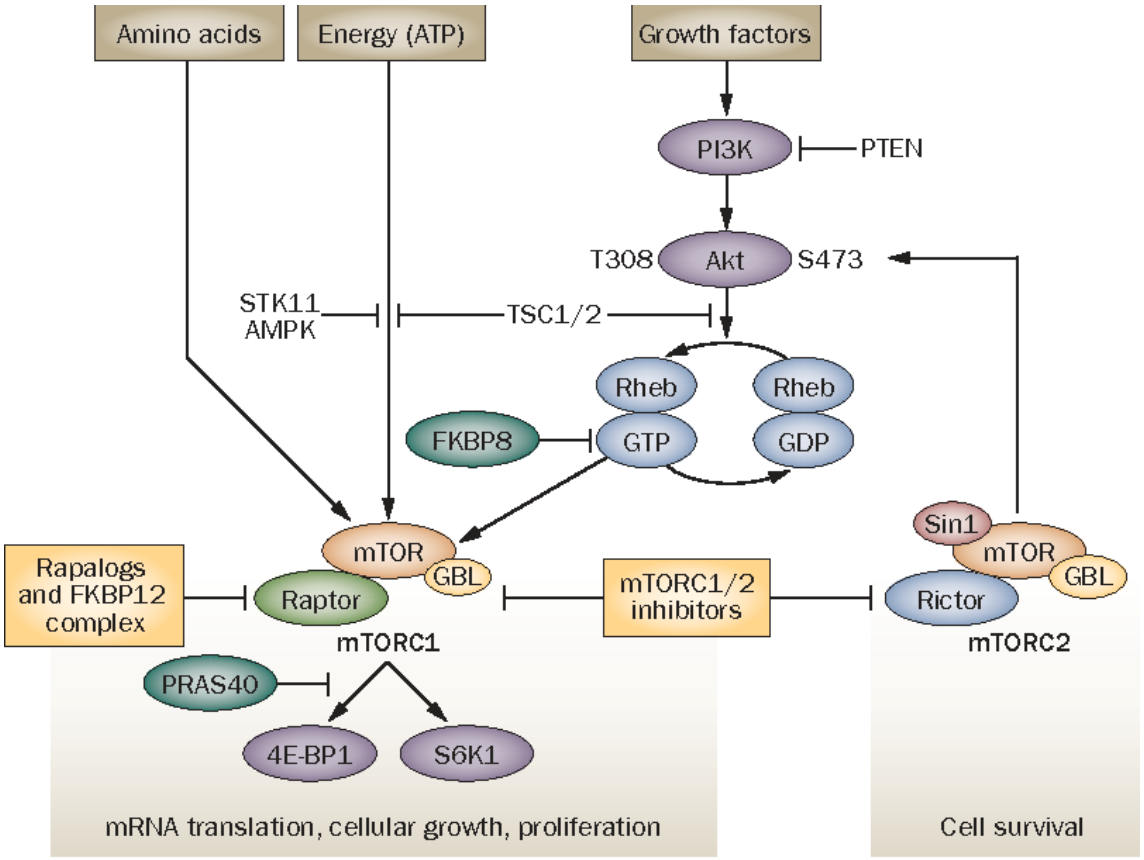

Figure 3. Overview of the PI3K/AKT/mTOR signaling pathway. mTOR signaling pathways. mTOR forms complexes with other proteins, including Raptor (forming mTORC1) or Rictor (forming mTORC2). ATP, amino acids and signals from the PI3K/Akt pathway modulate mTOR function. Activation of PI3K and Akt inhibits hamartin and tuberin repression of Rheb, which leads to mTORC1 activation and phosphorylation of S6K1 and 4E-BP1. Akt is pivotal in mTOR signaling, as it is both an upstream activator of mTORC1 and downstream effector of mTORC2. Negative regulators of mTOR include FKBP8, which prevents Rheb from activating mTORC1, and PRAS40, which competes with Raptor for binding to S6K1 and 4E-BP1. When intracellular ATP is depleted relative to AMP, AMPK and its upstream regulator STK11 phosphorylate tuberin, which inactivates Rheb and mTORC1 signaling. Hypoxia and low amino acid levels also negatively regulate mTOR. Rapalogs associate with FKBP12 and preferentially disrupt mTORC1 whereas small-molecule mTOR kinase inhibitors target both mTOR complexes. Abbreviations: AMPK, AMP-activated kinase; 4E-BP1, eIF4E-binding protein 1; FKBP12, FK506 binding protein 12; GBL, G protein beta subunit-like; mTORC, mammalian target of rapamycin complex; PI3K, phosphatidylinositol 3-kinase; PRAS40, proline-rich Akt1 substrate 1; PTEN, phosphatase and tensin homolog deleted on chromosome 10; S6K1, p70 S6 kinase 1; Sin1, stress activated protein kinase interaction protein 1; STK11, serine/threonine-protein kinase 11; TSC, tuberous sclerosis complex (Dancey J. 2010).

The BRAF V600E point mutation consists of the replacement of a thymine with adenine at nucleotide 1796, with consequent amino acid substitution in the codon 600 of a valine with glutamate (Nicolaides T.P. et al., 2011). This mutation occurs at the level of the kinase domain, at the activation loop (A loop) or at the loop to which ATP (P loop) binds,

causing a conformational change of the BRAF protein that becomes constitutively active. The highest frequency of the V600E mutation was found in PXAs (66%) and GGs (18%), while in PAs it represents 9% of cases (Schindler G. et al., 2011). As for the most common fusion of pLGGs, this occurs between BRAF and its centromeric gene, KIAA1549, following which transcription of different messengers is obtained after "alternative splicing". This in-frame fusion of KIAA1549-BRAF has been reported in 80% of sporadic PAs (Jones D.T. et al., 2009). Most of these KIAA1549-BRAF fusions occur between exon 16 of KIAA1549 and exon 9 of BRAF. However, there are at least six possible exon couplings for the KIAA1549-BRAF fusion (15: 9, 16:11, 16:10, 15:11, 17:10, 18:10) and in all the N-terminal of BRAF is replaced by that of KIAA1549. This results in a constitutive activation of the MAPK pathway, as the self-inhibiting N-terminal BRAF domain is lost while the C-terminal kinase domain is maintained (Jones D.T. et al., 2008; Jones D.T. et al., 2009). Other mutations, such as FGFR1 alterations, are mainly expressed only by specific pLGGs subtypes, such as DNET (Qaddoumi I. et al., 2016). Along with the abovementioned dysregulated MAPK/ERK signaling (Jacob K. et al., 2011; Raabe EH. et al., 2011; Selt F. et al., 2017), aberrant activation of the PI3K/AKT signaling pathway is also a well-documented feature of gliomas, which has also been described in pLGGs (Zhang J. et al., 2013; Mueller S. et al., 2012; Hütt-Cabezas M. et al., 2013). In some cases, its dysregulation has been linked to genetic, such as *BRAF* fusions, *FGFR1* duplications and *MYB* rearrangements (Sturm D. et al., 2017), or epigenetic modifications, but in many cases the mechanism underlying PI3K/AKT pathway activation is still unknown.

2.2 MircoRNAs

2.2.1 MicroRNAs biogenesis

MicroRNAs (miRNAs) are short (20–23-nucleotide), endogenous, single-stranded RNA molecules that regulate gene expression at post-transcriptional level, by binding to sequences complementary to 3 'UTR (3' untranslated region) of the target mRNA (Winter J. et al., 2009). The microRNA processing pathway has long been viewed as linear and universal to all mammalian microRNAs. This canonical maturation includes the production of the primary microRNA transcript (pri-miRNA) by RNA polymerase II or III and cleavage of the pri-miRNA by the microprocessor complex Drosha–DGCR8 (Pasha)

in the nucleus. The resulting precursor hairpin, the pre-miRNA, is exported from the nucleus by Exportin-5–Ran-GTP. In the cytoplasm, the RNase Dicer in complex with the double-stranded RNA-binding protein TRBP cleaves the pre-miRNA hairpin to its mature length. The functional strand of the mature microRNA is loaded together with Argonaute (Ago2) proteins into the RNA-induced silencing complex (RISC), where it guides RISC to silence target mRNAs through mRNA cleavage, translational repression or deadenylation, whereas the passenger strand is degraded, Figure 4 (Lin S. et al., 2015).

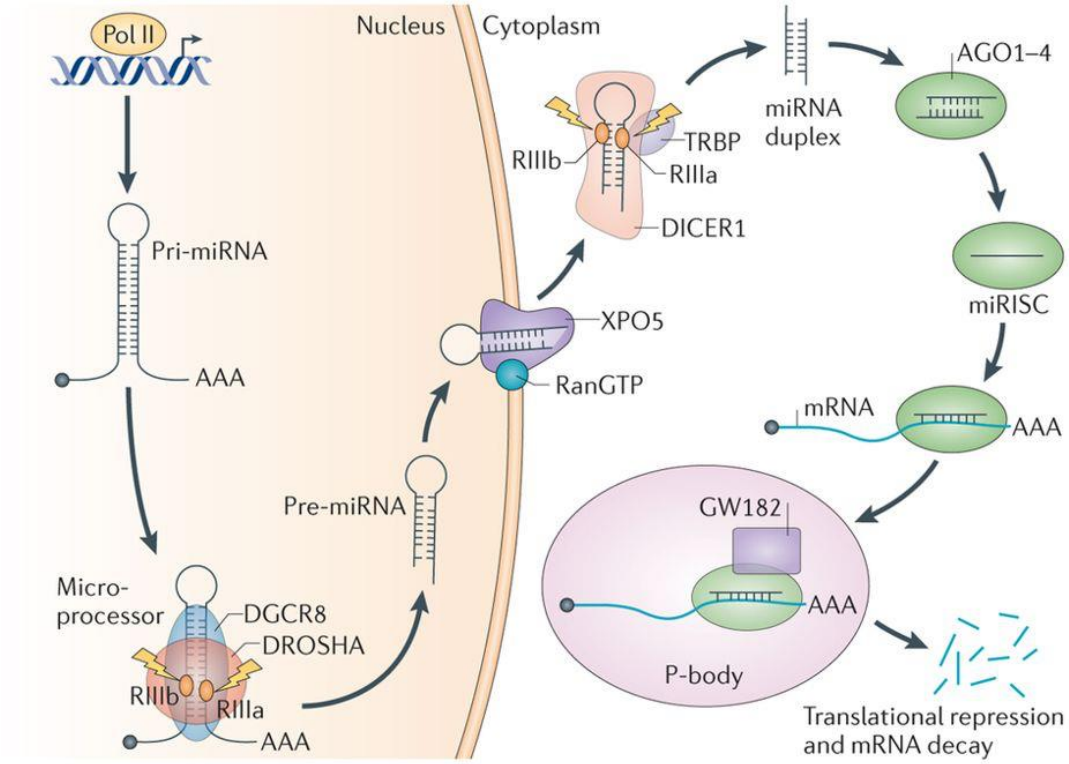

Figure 4. MicroRNA (miRNA) genes are transcribed as primary miRNAs (pri-miRNAs) by RNA polymerase II (Pol II) in the nucleus. The long pri-miRNAs are cleaved by Microprocessor, which includes DROSHA and DiGeorge syndrome critical region 8 (DGCR8), to produce the 60–70-nucleotide precursor miRNAs (pre-miRNAs). The pre-miRNAs are then exported from the nucleus to the cytoplasm by exportin 5 (XPO5) and further processed by DICER1, a ribonuclease III (RIII) enzyme that produces the mature miRNAs. One strand of the mature miRNA (the guide strand) is loaded into the miRNA-induced silencing complex (miRISC), which contains DICER1 and Argonaute (AGO) proteins, directs the miRISC to target mRNAs by sequence complementary binding and mediates gene suppression by targeted mRNA degradation and translational repression in processing bodies (P-bodies). TRBP, transactivation-responsive RNA-binding protein (Lin S. et al., 2015).

MicroRNAs and their targets constitute remarkably complex regulatory networks as a single microRNA can bind and regulate many different mRNAs and, conversely, different

microRNAs can cooperatively bind to and control a single target mRNA (Lewis et al, 2003).

2.2.1 MicroRNAs and cancer

Many cellular pathways are affected by the regulatory function of microRNAs; the most prominent of these pathways control developmental and oncogenic processes. The first evidence of the involvement of microRNAs in human cancer derived from studies on chronic lymphocitic leukemia (CLL), particularly in an attempt to identify tumour suppressors at chromosome 13q14, frequently deleted in CLL. Dr. Croce's group reported that rather than along with containing a protein coding tumour suppressor gene, this critical region contains in fact two microRNA genes, miR-15a and miR-16-1, expressed in the same polycistronic RNA. This result provided the first evidence that microRNAs could be involved in the pathogenesis of human cancer as the deletion of chromosome 13q14 caused the loss of these two microRNAs (Calin G.A. et al, 2002). Later, many groups of researchers identified the role of different microRNAs in human neoplasms, for example the amplification of the miR-17-92 cluster, strongly stimulated by c-Myc in B-cell lymphomas and lung tumours, hinders the expression of tumour suppressors and therefore promotes cancer progression. During tumour development, microRNAs can be subject to "gain of function" mutations, when mutations cause an aberrant over-expression of microRNA, or "loss of function" if, on the other hand, the expression or normal function physiological microRNA fails. For this reason some microRNAs are identified as oncogenes or oncosuppressors, depending on how their expression varies in human neoplasms and their function in cellular processes linked to the gene targets they regulate (Iorio MV. et al., 2005). The aberrant biogenesis of microRNAs in cancer can occur at different stages:

• At the transcriptional level, through specific transcription factors;

• Genetic alterations, such as amplification or loss of heterozygosity (LOH) affecting gene loci of microRNAs;

• Epigenetic modifications, for example methylation of CpG islands in tumour suppressor promoter regions.

2.2.3 MicroRNAs in pLGGs

The first microarray analysis on the expression profile of microRNAs in pLGGs was performed by the Birks group in 2011 on frozen tumour tissue samples. This analysis had identified three microRNAs (miR-129, miR-142-5p and miR-25) differentially expressed in tumours compared to healthy controls (Birks D.K. et al., 2011). In 2013, Ho et al. analysed 43 PAs and from microarray analysis detected several downregulated microRNAs, including miR-124, miR-129, miR-138, miR-490, miR-7 and miR-873, and others upregulated, including miR-10b, miR-1260, miR-1274, miR-1288, miR-142, miR-143, miR-21, miR-92b, compared to controls (Ho C.Y. et al. 2013). Subsequently, Liu et al. analysed the expression pattern of microRNAs from eight astrocytoma samples, divided according to malignancy. Through microarray and qRT-PCR they reported several upregulated microRNAs, such as miR-21, miR-181, miR-1321, miR-1259, miR-24, miR-222; and downregulated, such as miR-128, miR-885, miR-99b, miR-204, miR-218, miR-26a. In addition to the analysis of microRNAs, they also proceeded to investigate possible gene targets and reported genes involved in the MAPK, Wnt/β-catenin and migration promoting receptor (EphB2) signaling pathway (Liu F. et al., 2013). Later, Eguía et al. evaluated microRNA expression levels in 57 PAs samples of Mexican children, which included tumours from I to IV grade of malignancy. MiR-124-3p and miR-128-1 were downregulated in all astrocytomas compared to healthy brain tissues and this reduction was much more evident in grade IV astrocytomas. Furthermore, miR-128-1 levels were higher in infratentorial tumours than in supratentorial cases and miR-221-3p expression was higher in tumours without relapses and surviving patients (Eguía A.P. et al. 2014). Jones et al. in 2015 focused on the differential expression of microRNAs in a cohort of 57 pLGGs samples. In PAs, compared to controls, they found a significant upregulation of miR-542-5p, miR-542-3p, miR-503, mir-450, miR-224, miR-146a and miR-34a. Target analysis of these upregulated microRNAs revealed regulators of the MAPK signaling pathway, such as KRAS, MEK1 or ERK1. MicroRNAs such as miR-21 and miR-146a presented instead gene targets belonging to NF-KB signaling (Jones T.A. et al., 2015). In 2016 Braoudaki et al. analysed the expression profile of microRNAs in a DNET cohort. 120 differentially expressed microRNAs were identified between these tumours and healthy brain tissue and two of these microRNAs (miR-1909 * and miR-3138) have been proposed as biomarkers capable of distinguishing DNETs from healthy subjects

(Braoudaki M. et al., 2016). More recently, Bongaarts et al. demonstrated the role of two microRNAs (miR-519d and miR-4758) in the regulation of the intracellular PI3K/AKT/p21 signaling pathway in low-grade pediatric brain tumours associated with epilepsy, which include GGs and DNETs, and proposed these two microRNAs as biomarkers able to distinguish GGs from DNETs (Bongaarts A. et al., 2018). The abovementioned studies highlight the fact that microRNAs in pLGGs play an important role in the regulation of a great variety of genes and, consequently, of multiple signaling pathways. This can be exploited in the early detection of diseases, in risk assessment and in innovative therapeutic strategies.

3. Aim of work

Pediatric low grade gliomas (pLGGs) are the most frequent brain tumours and with heterogeneous clinical and histological aspects. About 40% of patients with pLGGs can be surgically treated by complete resection of the tumour. For tumours that occur at the supratentorial level, however, total surgical resection is difficult to obtain and, following partial tumour resection, patients often experience disease recurrence as well as suffering from important co-morbidities due to the late effects of treatment. In the field of oncology, microRNAs have assumed considerable importance both for their function as regulators of gene expression, acting as oncogenes and/or onco-suppressors, and as biomarkers of disease.

Thus, aim of this project has been to analyse a series of pLGGs samples to determine their microRNA profile and subsequently to focalize the study on deregulated microRNAs in supratentorial pLGGs subgroup, which have the poorest clinical outcomes, to find molecular aspects of pathogenic interest.

4. Materials and methods

Unless otherwise stated, commercially available products were used according to the manufacturer's instructions/protocols.

4.1 Tumour samples and controls

MicroRNA profiling was performed with quantitative PCR (qPCR) (as described below) on RNA extracted from snap-frozen tumour tissue samples from 45 patients (aged 1–16 years) with pLGGs. All underwent surgery at the Bambino Gesù Children's Hospital in Rome or the Gaslini Institute in Genoa between 2014 and 2016. The clinical and pathological features of each case are summarized in Table 5. The study was approved by the ethical committees of the competent structures and the families of the patients signed the informed consent for participation in the study. RNA and DNA used for the analyses were extracted from tumour samples with pathologist-confirmed tumour cell contents of 80% or more. For control purposes, we profiled eight samples (three + a pool of five) of non-neoplastic brain tissue purchased from Ambion-Life Technology (Thermo Scientific, Wilmington, MA, USA) (n = 1: AM7962, Human Brain Total RNA) or Biochain Institute (Newark, CA, USA) (n = 7: R1234035-50, Total RNA-Human Adult Normal Tissue-Brain; R1234035-P, Total RNA-Human Adult Normal Tissue-5 Donor Pool-Brain; R1234035-50, Total RNA-Human Adult Normal Tissue-Brain) and 28 samples (four + a pool of 24) of non-neoplastic brain cerebellum purchased from Biochain Institute (n = 4: R1234039-50, Total RNA-Human Brain cerebellum) or Clontech Laboratories (Takara Bio USA Inc., Shiga, Japan) (n = 1: 636535, Total RNA-Human Brain cerebellum-24 Donor Pool-Brain). MicroRNA profiles for the pLGGs were also compared with profiles previously reported by our group for 13 pHGGs, which had been collected between 2005 and 2010 from patients aged from 3 to 17 years (Miele E. et al., 2013). To ensure the comparability of these two cohorts, we reanalysed the microRNA profiles originally reported for the pHGGs using the same normalization procedure and statistical methods employed for comparing the pLGGs with healthy brain tissues, as reported below. For functional studies, we established short-term cultures of pLGG cells isolated from four primary tumours resected at Bambino Gesù Children's Hospital (Rome) in 2016 (Table 6). We deliberately selected tumours with non-PA histology, since the biology of these

pLGGs has been much less thoroughly explored than that of PAs. We also limited our analysis to supratentorial pLGGs, which are associated with lower miR-139-5p levels, lower resectability rates and worse outcomes than their infratentorial counterparts (Mueller S. et al., 2012).

4.2 Patient-derived primary pLGG cell cultures

4.2.1 Culture and characterization

Human pLGG samples, were collected immediately after resection and placed in Hank's Balanced Salt Solution (HBSS) supplemented with 0.5% glucose and penicillin-streptomycin. The tissues were triturated with a serological pipette. DNAse I was added (final concentration 0.04%) and left for 20 min. Cell aggregates were then mechanically disrupted with pipettes of decreasing bore size. The single-cell suspension thus obtained was then centrifuged, and the cells suspended in NHA complete medium (Lonza, Basel, CH), counted and plated at a density of 160,000/mL, Figure 5.

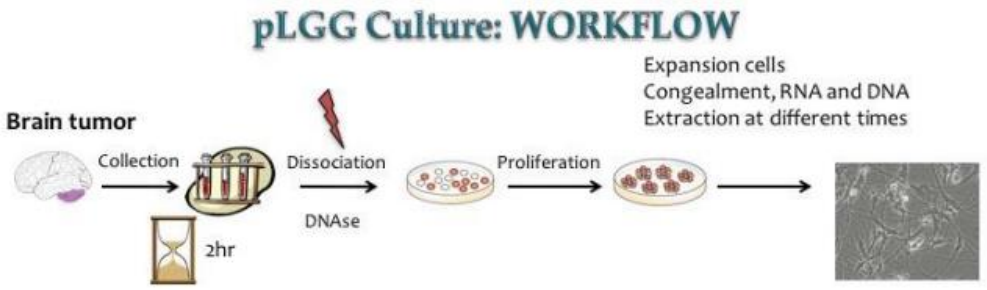

Figure 5. Protocol for Patient-derived primary pLGG cell cultures.

Prior to use in experiments, isolated primary pLGG cells underwent quality control assays to ensure they were reliable pLGG models. To this end, we verified that the BRAF status of each cell line was identical to that of the parent tumour (as described below in Analysis of BRAF status). For the three primary pLGG cells whose primary tumour did not show any genetic alteration on the BRAF gene, we compared methylation profiles to verify similarity between the primary cell line and the parental tumour. Immunofluorescence staining (described below) was used to confirm that the cells' histotype-specific glial/neuronal cell biomarker profile was consistent with those described in the literature (Louis D.N. et al., 2007, Luyken C. et al., 2004). The percentage of senescent cells was also evaluated by staining for Senescence-associated b-

galactosidase (SA-b-gal, described below). Cultures with SA-b-gal-positivity rates of 60% or more were excluded from experimentation. During the study, cells were discarded after a maximum of eight passages (about 30 days of culture) or when SA-b-gal-positivity rates reached 60%.

4.3 Histology

Formalin-fixed paraffin-embedded (FFPE) samples of each of the 45 pLGGs used in the study were sectioned (3µm) and stained with haematoxylin and eosin for histology. All tumour diagnoses were then confirmed by consensus decision of three neuropathologists (F.G., M.A. and F.D.C.) using the WHO classification criteria (Louis D.N. et al., 2016).

4.4 RNA extraction of pLGG tissues and cells

Trizol Reagent (Invitrogen, Thermo Scientific, CA, USA) was used to isolate total RNA from fresh-frozen pLGG tissue samples and patient-derived pLGG cell lines. To increase the RNA yield of the tissue samples, we added 250 µg glycogen (Invitrogen, Thermo Scientific, CA, USA) for each milliliter of Trizol. Total RNA quantity and quality were evaluated with a Nanodrop ND-100 spectrophotometer (Thermo Scientific). For each sample, we reverse-transcribed total RNA (500 ng to 1µg) using a high-capacity cDNA reverse transcription kit (Applied Biosystems,Thermo Scientific).

4.5 Analysis of BRAF status

Each of the 45 pLGGs and the three patient-derived pLGG cell lines were analysed for the two most common genetic alterations found in these tumours – namely, the BRAF V600E point mutation (V600E) and the KIAA1549:BRAF fusion gene [including the three most frequent variants: KIAA1549-BRAF exon 16-exon 9 (K16B9), KIAA1549-BRAF exon 16-exon 11 (K16B11), and KIAA1549-BRAF exon 15-exon 9 (K15B9)].

BRAF fusion analysis. BRAF fusion analysis was performed on tumour cDNAs with the Applied Biosystems Viia7 real-time qPCR (RT-qPCR) System, as described by Tian et al. (Tian Y. et al., 2011) and validated by PCR based Sanger sequencing through amplification with specific pairs of primers flanking the fusion point between the KIAA1549 (in exon 15 or 16) and BRAF (in exon 9 or 11) genes, as described by Jones et al. (Jones D.T. et al., 2008). The purified PCR products were sequenced on an ABI 3130

XL DNA analyser (Applied Biosystems) using the BigDye Terminator v1.1 cycle sequencing kit (Applied Biosystems) and the forward or reverse primer used to perform the PCR. The primer sequences were as follows: KIAA1549 exon 15: 5'-CGG AAA CAC CAG GTC AAC GG-3'; KIAA1549 exon 16: 5'-AAA CAG CAC CCC TTC CCA GG-3'; BRAF exon 9: 5'-CTC CAT CAC CAC GAA ATC CTT G-3'; BRAF exon 11: 5'-GTT CCA AAT GAT CCA GAT CCA TTC-3'.

BRAF V600E mutation. DNA was extracted from fresh frozen samples and patient-derived pLGG cell lines using the QIamp DNA mini kit (Qiagen Inc., Valencia, CA, USA). Quantity and quality were evaluated with a Nanodrop ND-1000 spectrophotometer (Thermo Scientific). RT-qPCR was performed, as described by Diniz et al. (Diniz M.G. et al., 2015), using TaqMan probes (Life Technologies, Waltham, MA, USA): BRAF_476_mu, which detects T>A transversion at position c.1799, and the reference-gene probe BRAF_rf. Threshold cycle (Ct) values were analysed using Mutation Detector™ Software (Life Technologies). Genomic DNA extracted from BRAF V600E and BRAF wild-type colon cancer cell lines, kindly provided by Prof. Matilde Todaro (University of Palermo), were used as positive and negative controls, respectively.

Table 5. Clinical-pathological features of the 45 pLGG cases subjected to microRNA expression profiling.

Sample	**Age at diagnosis (y)**	**Sex**	**Histology**	**WHO grade**	**Location**	**BRAF alterations[a]**
P5	3	M	AG	II	Supra	WT
P38[b]	12.3	M	AG	I	Supra	WT
P3[b]	9	F	DNET	I	Supra	WT
P11	10	F	DNET	I	Supra	WT
P16[b]	5.8	M	DNET	I	Supra	WT
P32	8.4	F	DNET	I	Supra	WT
P8	7.6	F	GG	I	Supra	WT
P18[b]	14.7	F	GG	I	Supra	V600E

P19	4.5	M	GG	I	Infra	V600E
P22	8	F	GG	I	Infra	K16B9
P26	7	F	GG	I	Supra	WT
P29	11.3	M	GG	I	Infra	WT
P36	5.5	M	GG	I	Infra	K15B9
P41	1.6	M	GG	I	BS	WT
P33	9.1	F	GNT	I	Infra	K15B9
P1	15	F	PA	I	Infra	WT
P2	1	F	PA	I	Infra	K16B9
P4	12	M	PA	I	Infra	WT
P6	9	M	PA	I	Supra	K16B9
P7	6.1	F	PA	I	Infra	K16B9
P9	1.9	F	PA	I	Infra	K15B9
P10	16.2	M	PA	I	Infra	WT
P12	3.8	M	PA	I	Infra	K16B9
P13	5.7	M	PA	I	Infra	WT
P14	1.3	F	PA	I	Infra	WT
P15	10	F	PA	I	Infra	WT
P17	12	M	PA	I	Infra	WT
P20	4.4	F	PA	I	Infra	K16B9
P21	10	M	PA	I	Supra	WT
P23	11	F	PA	I	Infra	WT
P24	3	M	PA	I	Supra	K16B9
P25	9.4	F	PA	I	BS	K16B9
P27	10	M	PA	I	Infra	K16B9
P28	7	F	PA	I	BS	WT
P30	6.8	F	PA	I	Supra	K16B11
P31	10.2	M	PA	I	Infra	K16B9

P34	5	M	PA	I	Supra	WT
P35	7.5	M	PA	I	Infra	K16B9
P37	3.2	M	PA	I	Supra	K15B9
P39	6.6	M	PA	I	Supra	WT
P40	1.4	M	PA	I	Infra	K16B9
P42	3.3	M	PA	I	Infra	WT
P43	1.8	F	PA	I	Infra	WT
P44	3.6	M	PA	I	Supra	K15B9
P45	3.1	M	PA	I	Infra	V600E

Abbreviations: AG, angiocentric glioma; BS, brain stem; DNET, disembryoplastic neuroepithelial tumour; GG, ganglioglioma; GNT, glioneruonal tumour; Infra, infratentorial; PA, pilocytic astrocytoma; pLGG, pediatric low-grade glioma; Supra, supratentorial; WT, Wild Type for BRAF screening.

[a] BRAF screening was limited to the V600E point mutation and three gene fusions (KIAA1549-BRAF exon 16-exon 9 [K16B9], KIAA1549-BRAF exon 16-exon 11 [K16B11], KIAA1549-BRAF exon 15-exon 9 [K15B9]).

[b] Primary pLGG cell lines were derived from these tumours (see Table 6)

Table 6. Clinical-pathological features of patient-derived primary pLGG cell lines**.**

Sample	**Parental Tumour**	**Age at diagnosis**	**Sex**	**Histology**	**Location**	**BRAF alterations[a]**	
						Tumour tissue	**Isolated cells**
pLGG1	P38	12.3	M	AG	Supra	WT	WT
pLGG2	P3	9	F	DNET	Supra	WT	WT
pLGG3	P16	5.8	M	DNET	Supra	WT	WT
pLGG4	P18	14.7	F	GG	Supra	V600E	V600E

Abbreviations: AG, angiocentric glioma; DNET, disembryoplastic neuroepithelial tumour; GG, ganglioglioma; NS, not screened; pLGG, pediatric low-grade glioma; Supra, supratentorial; WT, Wild Type for BRAF screening.

[a] BRAF screening was limited to the V600E point mutation and three gene fusions (KIAA1549-BRAF exon 16-exon 9 [K16B9], KIAA1549-BRAF exon 16-exon 11 [K16B11], KIAA1549-BRAF exon 15-exon 9 [K15B9]).

4.6 MicroRNA profiling and data analysis

MicroRNA expression profiling was performed on the pLGG tumours using RT-qPCR with Taqman Low Density Array (TLDA) microfluidic cards (Human miR v3.0, Applied Biosystems), which detect the 754 best characterized members of the human microRNA genome. Each reverse transcriptase reaction was performed with specific primers according to Applied Biosystems protocols. The same method had been used to profile the pHGGs in (Miele E. et al., 2013). Statistical analysis was performed with StatMinerTM software, v. 5.0 (Integromics TM, Granada, Spain). MicroRNA expression levels were normalized by using the global expression normalization method and the comparative threshold cycle method was used to calculate the relative microRNA expression. MicroRNAs with Ct values > 33 were excluded. Differential expression between groups was assessed with the Limma test, and p values < 0.05 were considered to be statistically significant. A single-assay qPCR for assessment of miR-139-5p expression (Code:002289) was carried out in triplicate using the TaqMan Individual microRNA assays (Applied Biosystems), as previously described (Miele E. et al., 2013). Information regarding microRNA clusters was obtained from miRBase v.21 (http://www.mirbase.org/) (Griffiths-Jones S. et al., 2007)

Validated targets of hsa-miR-139-5p were identified by interrogation of the miRTarBase (http://mirtarbase.mbc.nctu.edu.tw/; (Chou C-H. et al., 2015)) and literature reports (Dai S. et al., 2015; Yue S. et al., 2015).

4.6.1 MicroRNAs clustering analysis

Dendrograms and heat maps were generated with the use of R (http://www.r-project.org/) using differentially expressed microRNAs as input. The Bray-Curtis method and the average linkage were used in hclust to cluster the samples and heatmap.2 to generate the heat maps (Suzuki R. et al.,2006).

4.6.2 DIANA mirPath analysis

The microRNAs that were differentially expressed in pLGGs (vs. non-neoplastic brain tissue controls) were loaded into the DIANA mirPath tool (http://snf-515788.vm.okeanos.grnet.gr/) Vlachos IS. Et al., 2015) for microRNA pathway analysis. MicroRNAs that were significantly dysregulated in the tumours were then analysed to identify their putative targets.

4.7 Cell treatments

Synthetic miR-139-5p (miRIDIAN microRNA code: C-310568-07; Dharmacon, Cornaredo, Milan, Italy) or negative control (miRIDIAN microRNA negative control code: CN-001000-01; Dharmacon) were transfected into pLGG primary cells at 20 nM using HiPerFect transfection reagent (Qiagen Inc.) for 48h. miR-139-5p overexpression was confirmed by single assay qRT-PCR. For pharmacological inhibition of PI3K, LY294002 was purchased from Sellekchem, dissolved in DMSO, and stored until used in aliquots at -80°C as 50 mM stock solutions. LY294002 and controls (CTRL) (0.1% DMSO) were diluted in culture medium just before use. After 30 min of treatment with 50 μM LY294002, cells were shifted in normal culture medium for a recovery period of 48h. Cell growth was evaluated after 48h by trypan blue exclusion assay. Specifically, the number of cells that did not take up trypan blue (viable cells) was counted both after transfection of synthetic miR-139-5p or negative control. The number of cells that took up trypan blue (nonviable cells) was counted. Each sample was measured in triplicate and repeated at least three times.

4.8 DNA methylation array data generation

DNA methylation profiling using the Illumina Infinium HumanMethylation EPIC BeadChip array was performed according to the manufacturer's instructions in collaboration with the Genetics and Rare Diseases Research Division, Bambino Gesù Children's Hospital, Rome, Italy. In detail 250 ng of DNA was used as input material for fresh frozen tissue and primary cell line samples (after about 15 days of culture). t-Distributed stochastic neighbor embedding (TSNE) analysis was conducted as previously described (Sturm D. et al., 2016). Basic array processing and clustering analysis were performed using Illumina GenomeStudio V2011.1 (Methylation Module version 1.9.0, content descriptor version 1.2) (https://www.illumina.com/techniques/microarrays/array-data-analysisexperimental-design/genomestudio.html) (Illumina, Inc., San Diego, CA, USA). Signal intensities were obtained without background subtraction and normalized to internal controls. Beta-values were used for downstream methylation analyses.

4.9 Immunofluorescence studies

Immunofluorescence studies were performed according to standard procedures, as reported elsewhere (Ronci M. et al., 2015). Primary pLGG cells were plated on glass coverslips and fixed with 4% paraformaldehyde (PFA) for 10 min at room temperature (RT). Fixed cultures were permeabilized and blocked for 30 min with 5% donkey serum (DS) and 0.1% Triton X-100 (Sigma-Aldrich, St. Louis, MO) in phosphate buffered saline (PBS). Cells were then incubated overnight with the following primary antibodies: anti-glial fibrillary acidic protein (GFAP, 1:200, Cell Signaling Technology, Danvers, MA), anti-vimentin (1:100, Abcam, Cambridge, UK), anti-S100 (1:100, Sigma-Aldrich, St. Louis, MO), anti-NeuN (1:100, Merck Millipore, Darmstadt, GE), anti-synaptophysin (1:100, Merck Millipore, Darmstadt, GE) diluted in PBS with 5% DS. Secondary antibodies conjugated with Alexa Fluor 488 or 594 (Thermo Fisher Scientific, MA, USA) were diluted 1:400 and 1:200, respectively, in PBS with 5% DS and incubated with the specimens for 1h at RT. Nuclei were counterstained with Hoechst reagent. After washing, slides were mounted using anti-fade reagent (Prolong Gold, Thermo Fisher Scientific, MA, USA). Images were acquired using a FV1200 MPE laser scanning confocal microscope (Olympus) with a UPlanSAPO 40x/0.95 NA objective. Imaris 8.1 software (Bitplane, Zürich, CH) was used for image-processing. For image analysis, 200 cells resulted from five fields from three independent experiments were examined and the percentage of positive cells for each marker was evaluated by dividing the number of positive cells on the total number of cells in each field.

4.10 Senescence-Associated-β-galactosidase activity

SA-β-gal activity was assessed as described in Debacq-Chainiaux (Debacq-Chainiaux F. et al., 2009) with minor modifications. Briefly, cells were fixed with 3.6% of formaldehyde in PBS for 4 min at RT. Fixed cells were washed and incubated overnight with freshly prepared staining solution at 37°C in the absence of CO_2. The cells were washed, and coverslips were mounted in antifade medium (Dako Fluorescence mounting medium, Agilent Technologies, Santa Clara, CA). Images were acquired using a Leica DM2500 microscope (Leica Microsystems, Wetzlar, Germany) with a 20x/0.40 NA objective. Pictures were taken using the ISCapture software and processed with Adobe Photoshop (Mountain View, CA) to adjust brightness and contrast. The percentage of positive cells

was evaluated by dividing the number of blue cells on the total number of cells in the field (Jacob K. et al., 2011).

4.11 Western Blotting

Western blotting analysis was performed according to standard procedures, as reported elsewhere (Po A. et al., 2017). Blots were incubated with primary antibodies: rabbit anti-phospho-Akt (Ser473), rabbit anti-Akt, rabbit anti-phospho-p70 S6 kinase (Thr389), rabbit anti-p70 S6 kinase (Cell Signaling Technology, Danvers, MA), and mouse anti-GAPDH (Abcam, Cambridge, UK). HRP-conjugated secondary antisera (Santa Cruz, Biotechnology) were added, and binding was visualized by enhanced chemiluminescence (Perkin Elmer, MA, USA). Images were acquired with the BioRad ChemiDoc MP Imaging System (BioRad, Hercules, CA). BioRad associated Image Lab Software was used to perform densitometric analysis. Values are expressed as fold changes relative to GAPDH, used as internal control.

4.12 Statistical Analysis

Data reported in this paper are the means ± SD of at least three independent experiments each performed in triplicate. Unpaired t-test and Paired t-test were performed wherever appropriate using GraphPad Prism Software version 6.0 (La Jolla, CA, USA), P values < 0.05 were considered to be statistically significant.

5. Results

5.1 Genetic alterations of the pLGG cohort

The evaluation of the BRAF V600E point mutation (V600E) and the KIAA1549:BRAF fusion gene in tumour samples and in cells showed KIAA1549:BRAF fusion genes common, in accordance to literature (Zhang J. et al., 2013). Specifically, the K16B9 variant – the one most frequently encountered – was present in 18 (27%) pLGGs, most of which (13, 52%) were infratentorial. BRAF fusions were less common in the supratentorial tumours [5/18 (29%)]. Three pLGGs harboured the BRAF V600E point mutation (two infratentorial and one supratentorial).

These results together with other clinical and pathological features of the 45 primary pLGGs analysed are summarized in Table 5. Thirty (67%) of the tumours were PAs, eight (18%) were gangliogliomas (GGs), four (9%) were DNETs, two (4%) were AGs and one (2%) was a glioneuronal tumour. Patients' age at diagnosis ranged from 1 to 16 years (median 7 years; mean 7.1 years). Three were located in the brain stem (two PAs, one GG). The other 42 included comparable numbers of infratentorial (n = 25) and supratentorial (n = 17) tumours.

5.2 MicroRNA profiles of pLGGs

We measured the expression levels of 754 microRNAs in the 45 pLGGs described above and compared them with non-neoplastic brain (CTRL). The results were also compared with profiles previously reported by our group for 13 pHGGs (glioblastoma multiforme, n = 8; anaplastic astrocytoma, n = 5) (Miele E. et al., 2013). The TLDA analysis reported similar high detection rates in all the three tissue groups [474 (63%) of the 754 microRNAs were identified in pLGGs, 436 (58%) in pHGGs and 368 (49%) in CTRL]. The differentially expressed microRNAs (Tables 7 and 8) were plotted using hierarchical clustering, as reported in Figure 6.

Table 7. MicroRNAs displaying significantly upregulated expression in pLGG tissues relative to non-neoplastic brain (CTRL). Abbreviations: LFC, Linear Fold Change; Chr, Chromosome

microRNA	LFC	P-value	Part of cluster	Chr

hsa-miR-193a-3p	34.32	6.84E-03		
hsa-miR-378	30.16	1.26E-02		
hsa-miR-1275	19.21	5.39E-04		
hsa-miR-18a-5p	14.20	2.36E-05	17~92	13
hsa-miR-576-3p	13.90	2.22E-02		
hsa-miR-483-5p	10.28	3.13E-03		
hsa-miR-720	8.65	1.32E-04		
hsa-miR-550a-3p	8.61	9.25E-04	550a~550b	7
hsa-miR-636	8.15	4.08E-02		
hsa-miR-296-5p	7.08	3.38E-05	298~296	20
hsa-miR-337-5p	7.00	2.17E-02	493~136	14
hsa-miR-21-5p	6.83	3.09E-03		
hsa-miR-455-5p	5.14	1.14E-03		
hsa-miR-301a-3p	5.01	2.78E-05		
hsa-miR-661	5.00	1.85E-02		
hsa-miR-9-3p	4.80	2.92E-04		
hsa-miR-497-5p	4.66	9.14E-06	497~195	17
hsa-miR-1260a	4.17	1.23E-02		
hsa-miR-34a-3p	3.86	3.35E-03		
hsa-miR-571	3.75	4.75E-02		
hsa-miR-142-3p	3.61	8.50E-03	4736~142	17
hsa-miR-320b	3.60	4.56E-02		
hsa-miR-27a-3p	3.42	5.49E-04	23a~24-2	19
hsa-miR-99a-3p	3.19	1.53E-02	99a~let-7c	21
hsa-miR-155-5p	3.13	1.24E-02		

hsa-miR-34a-5p	2.97	9.34E-03		
hsa-miR-181c-5p	2.93	2.42E-02	181c~181d	19
hsa-miR-193a-5p	2.52	0.02		
hsa-miR-362-5p	2.36	9.19E-03	532~502	X
hsa-miR-374a-5p	2.31	1.31E-02	374a~545	X
hsa-miR-20a-5p	2.09	2.12E-02	17~92	13
hsa-miR-195-5p	2.04	3.86E-02	497~195	17
hsa-miR-20b-5p	1.94	3.38E-02	106a~363	X
hsa-miR-106b-5p	1.75	3.63E-02	106b~25	7

Table 8. MicroRNAs displaying significantly downregulated expression in pLGG tissues relative to non-neoplastic brain (CTRL). Abbreviations: LFC, Linear Fold Change; Chr, Chromosome

microRNA	**LFC**	**P-value**	**Part of cluster**	**Chr**
hsa-miR-129-1-3p	0.01	3.65E-03		
hsa-miR-485-5p	0.01	1.13E-02	379~656	14
hsa-miR-129-2-3p	0.01	1.27E-02		
hsa-miR-147b	0.01	2.05E-02		
hsa-miR-523-3p	0.03	4.69E-02	512-1~519a-2	19
hsa-miR-187-3p	0.04	3.82E-02		
hsa-miR-203a	0.04	7.74E-03	203a~203b	14
hsa-miR-522-3p	0.04	1.94E-02	512-1~519a-2	19
hsa-miR-582-5p	0.04	3.39E-02		
hsa-miR-153-3p	0.04	3.47E-02		
hsa-miR-184	0.05	2.04E-02		
hsa-miR-7-2-3p	0.05	1.05E-02	1179~3529	15

hsa-miR-770-5p	0.05	5.82E-03		
hsa-miR-139-5p	0.06	3.27E-04		
hsa-miR-133a-3p	0.06	3.12E-03		
hsa-miR-139-3p	0.06	6.83E-03		
hsa-miR-577	0.06	5.82E-03		
hsa-miR-517a-3p	0.06	2.17E-02	512-1~519a-2	19
hsa-miR-889-3p	0.06	1.16E-02	379~656	14
hsa-miR-584-5p	0.07	3.11E-02		
hsa-miR-425-3p	0.08	1.38E-02	191~425	3
hsa-miR-383-5p	0.08	4.15E-02		
hsa-miR-124-3p	0.08	1.15E-02		
hsa-miR-423-5p	0.09	3.16E-02	423~3184	17
hsa-miR-128-3p	0.10	1.53E-03		
hsa-miR-149-5p	0.11	8.06E-04		
hsa-miR-7-1-3p	0.11	5.30E-03		
hsa-miR-433-3p	0.12	0.02	493~136	14
hsa-miR-885-5p	0.14	3.23E-03		
hsa-miR-539-5p	0.14	4.44E-04	379~656	14
hsa-miR-487b-3p	0.14	7.05E-04	379~656	14
hsa-miR-218-5p	0.14	6.46E-03		
hsa-miR-874-3p	0.15	4.28E-02		
hsa-miR-628-3p	0.16	1.74E-02		
hsa-miR-628-5p	0.16	3.63E-03		
hsa-miR-495-3p	0.17	2.18E-02	379~656	14
hsa-miR-31-5p	0.18	4.70E-02		

hsa-miR-323a-3p	0.18	8.69E-04	379~656	14
hsa-miR-132-3p	0.18	2.99E-04	212~132	17
hsa-miR-138-5p	0.19	1.10E-02		
hsa-miR-330-3p	0.19	4.79E-05		
hsa-miR-95-3p	0.20	2.72E-03		
hsa-miR-491-5p	0.23	4.00E-05		
hsa-miR-410-3p	0.23	1.18E-03	379~656	14
hsa-miR-625-5p	0.24	1.25E-02		
hsa-miR-342-3p	0.26	5.29E-04	342~151b	14
hsa-miR-200c-3p	0.26	0.05	200c~141	12
hsa-miR-221-3p	0.28	4.44E-02	222~221	X
hsa-miR-625-3p	0.35	0.05		
hsa-miR-191-5p	0.38	4.25E-03	191~425	3
hsa-miR-126-3p	0.39	0.01		
hsa-miR-411-5p	0.39	1.36E-02	379~656	14
hsa-miR-655-3p	0.41	4.46E-02	379~656	14
hsa-miR-103a-3p	0.42	4.69E-03	103a~103b	20
hsa-miR-145-5p	0.43	3.25E-02	143~145	5
hsa-miR-339-3p	0.43	1.85E-02		
hsa-miR-125a-5p	0.43	1.01E-02	99b~125a	19
hsa-miR-324-5p	0.47	3.05E-02		
hsa-miR-454-3p	0.51	4.76E-02		

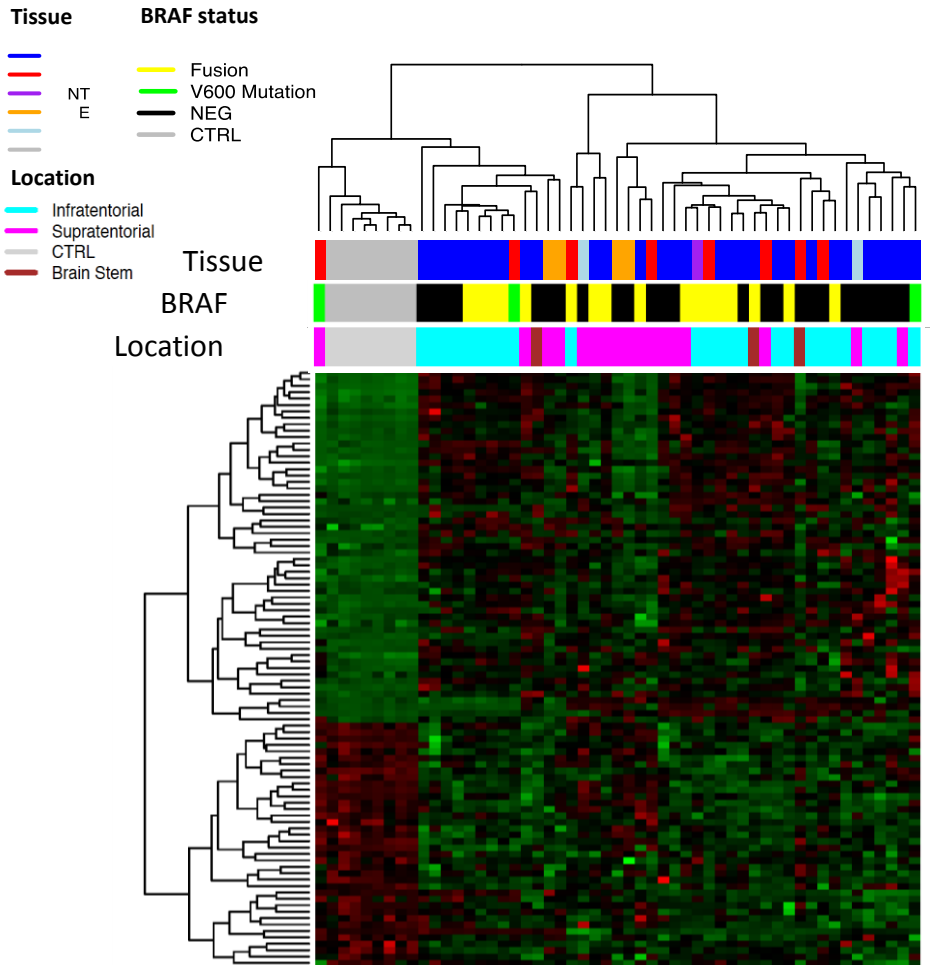

Figure 6. Hierarchical clustering of microRNAs displaying differential expression in pediatric low-grade gliomas (pLGGs) vs. nonneoplastic brain tissues (controls, CTRL). Hierarchical clustering of the 93 microRNAs differentially expressed in pLGGs vs. CTRL (grey) ($P < 0.05$) was performed and the Euclidean method was used to generate clusters on the basis of delta Ct values. Tissue: PA, pilocytic astrocytoma (blue); GG, ganglioglioma (red); GNT, glioneuronal tumour (purple); DNET, dysembryoplastic neuroepithelial tumour (orange); AG, angiocentric glioma (light blue). BRAF status was defined exclusively by the presence/absence of the V600E point mutation (green) and KIAA1549-BRAF fusion variants (yellow) (KIAA1549-BRAF exon 16-exon 9, KIAA1549-BRAF exon 16-exon 11, or KIAA1549-BRAF exon 15-exon 9). NEG, negative for all analysed mutations (black).

Some of the most striking alterations involved upregulation of microRNAs with documented oncogenic effects in many tumours (e.g. miR-21 and members of the miR-17-92 cluster) (Miele E. et al., 2013; Ho C-Y. et al., 2012;) down-regulation of microRNAs with reported oncosuppressive effects in various settings. The latter included miR-218 (Liu F. et al., 2013), miR-124 (Ho C-Y. et al., 2012), miR-487b (Ames HM. et al., 2017) and

miR-139-5p (Bao W. et al., 2011; Guo H. 2012; Wong C.C.L. et al., 2011; Mao R. et al., 2015; Qiu G. et al., 2015).

We further evaluated the microRNAs profiles of supratentorial and infratentorial tumours with respect to non-neoplastic brain or normal cerebellum as CTRL, respectively. Among supratentorial tumours, 69 micro-RNAs displayed significant tumour-related upregulation (n = 28) or down-regulation (n = 41) ($P < 0.05$) (Tables 9 and 10).

Table 9. MicroRNAs displaying significantly upregulated expression in supratentorial pLGGs with respect to non-neoplastic brain tissues (CTRL). Abbreviations: LFC, Linear Fold Change; Chr, Chromosome

microRNA	LFC	P-value	Part of cluster	Chr
hsa-miR-663b	46.20	3.99E-03		
hsa-miR-193a-3p	45.40	4.06E-02		
hsa-miR-378	31.89	1.60E-02		
hsa-miR-576-3p	17.65	2.46E-02		
hsa-miR-1275	17.02	2.57E-02		
hsa-miR-1225-3p	15.70	1.84E-02		
hsa-miR-337-5p	11.84	4.34E-02	493~136	chr14
hsa-miR-550a-3p	11.32	2.16E-03	550a~550b	chr7
hsa-miR-483-5p	10.93	1.05E-02		
hsa-miR-18a-5p	10.34	1.20E-02	17~92a-1	chr13
hsa-miR-720	9.61	3.38E-04		
hsa-miR-1233-3p	9.47	2.63E-02		
hsa-miR-106b-3p	6.43	3.29E-03	106b~25	chr7
hsa-miR-296-5p	6.05	4.68E-03	298~296	chr20
hsa-miR-29a-5p	5.96	4.09E-02	29b-1~29a	chr7
hsa-miR-661	5.95	9.16E-03		

hsa-miR-9-3p	5.53	9.78E-04		
hsa-miR-1260a	5.21	5.65E-04		
hsa-miR-301a-3p	5.15	8.52E-04		
hsa-miR-497-5p	4.69	9.94E-05	497~195	chr17
hsa-miR-99a-3p	3.88	3.27E-03	99a~let-7c	chr21
hsa-miR-455-5p	3.85	2.14E-02		
hsa-miR-34a-3p	3.42	2.33E-02		
hsa-miR-27a-3p	2.97	1.98E-02	23a~24-2	chr19
hsa-miR-19a-3p	2.81	0.042344329	17~92a-1	chr13
hsa-miR-362-5p	2.34	3.19E-02	532~502	chrX
hsa-miR-193a-5p	2.32	4.57E-02		
hsa-miR-181a-2-3p	2.14	3.68E-02	181a-2~181b-2	chr9

Table 10. MicroRNAs displaying significantly downregulated expression in supratentorial pLGGs with respect to non-neoplastic brain tissues (CTRL). Abbreviations: LFC, Linear Fold Change; Chr, Chromosome

microRNA	**LFC**	**P-value**	**Part of cluster**	**Chr**
hsa-miR-147b	0.006	7.85E-03		
hsa-miR-512-3p	0.007	1.93E-02	512-1~519a-2	chr19
hsa-miR-657	0.009	4.90E-02	1250~657	chr17
hsa-miR-523-3p	0.016	4.90E-02	512-1~519a-2	chr19
hsa-miR-485-5p	0.017	2.82E-03	379~656	chr14
hsa-miR-138-2-3p	0.017	8.82E-03		
hsa-miR-187-3p	0.024	2.58E-02		
hsa-miR-522-3p	0.044	3.44E-02	512-1~519a-2	chr19
hsa-miR-425-3p	0.044	1.17E-02	191~425	chr3

hsa-miR-423-5p	0.048	3.08E-03	423~3184	chr17
hsa-miR-577	0.083	2.72E-02		
hsa-miR-889-3p	0.100	4.60E-02	379~656	chr14
hsa-miR-184	0.108	3.24E-02		
hsa-miR-128-3p	0.114	2.69E-02		
hsa-miR-133a-3p	0.144	9.51E-03	1-2~133a-1	chr18
hsa-miR-139-5p	0.147	3.68E-02		
hsa-miR-203a	0.153	2.05E-02	203a~203b	chr14
hsa-miR-31-5p	0.156	3.28E-02		
hsa-miR-23b-3p	0.168	4.04E-02	23b~24-1	chr9
hsa-miR-654-5p	0.172	2.18E-02		
hsa-miR-495-3p	0.184	1.07E-02	379~656	chr14
hsa-miR-539-5p	0.198	5.34E-03	379~656	chr14
hsa-miR-149-5p	0.200	3.98E-02		
hsa-miR-138-5p	0.205	2.60E-02		
hsa-miR-7-1-3p	0.215	3.27E-02		
hsa-miR-487b-3p	0.215	1.56E-02	379~656	chr14
hsa-miR-625-5p	0.226	3.35E-02		
hsa-miR-132-3p	0.252	1.18E-02	212~132	chr17
hsa-miR-330-3p	0.266	0.011063144		
hsa-miR-628-5p	0.270	8.66E-03		
hsa-miR-323a-3p	0.270	3.29E-02	379~656	chr14
hsa-miR-410-3p	0.276	2.29E-02	379~656	chr14
hsa-miR-491-5p	0.277	7.67E-03		
hsa-miR-95-3p	0.332	3.67E-02		

hsa-miR-379-5p	0.345	1.59E-02	379~656	chr14
hsa-miR-342-3p	0.350	2.66E-02	342~151b	chr14
hsa-miR-200c-3p	0.362	3.55E-02	200c-141	chr12
hsa-miR-411-5p	0.412	0.024012639	379~656	chr14
hsa-miR-126-3p	0.418	3.91E-02		
hsa-miR-103a-3p	0.450	3.53E-02		
hsa-miR-191-5p	0.493	3.44E-02	191~425	chr3

Whereas in the analysis between infratentorial tumours and normal cerebellum 109 microRNAs displayed significant tumour-related up (n = 52) or down- regulation (n = 57) ($P < 0.05$) (Tables 11 and 12).

Table 11. MicroRNAs displaying significantly upregulated expression in infratentorial pLGGs with respect to normal cerebellum (CTRL). Abbreviations: LFC, Linear Fold Change; Chr, Chromosome

microRNA	**LFC**	**P-value**	**Part of cluster**	**Chr**
hsa-miR-875-5p	321.75	2.96E-02	875~599	chr8
hsa-miR-22-5p	123.85	8.14E-03		
hsa-miR-21-5p	112.16	5.83E-06		
hsa-miR-618	37.94	5.17E-03		
hsa-miR-24-2-5p	36.68	1.57E-03	23a~24-2	chr19
hsa-miR-34a-3p	32.05	5.74E-06		
hsa-miR-374b-5p	29.17	4.63E-03	374c~421	chrX
hsa-miR-335-5p	28.26	2.04E-04		
hsa-miR-137	25.38	2.73E-02	137~2682	chr1
hsa-miR-451a	23.21	2.99E-03	4732~451a	chr17
hsa-miR-142-3p	22.93	2.19E-04	4736~142	chr17

hsa-miR-18a-5p	19.80	3.89E-06	17~92a-1	chr13
hsa-miR-18b-5p	18.93	2.91E-02	17~92a-1	chr13
hsa-miR-221-3p	16.66	1.67E-03	222-221	chrX
hsa-miR-1183	14.26	3.87E-02		
hsa-miR-708-5p	13.78	7.78E-08		
hsa-miR-9-3p	11.04	2.96E-04		
hsa-miR-19b-3p	9.88	2.09E-03		
hsa-miR-144-5p	9.24	4.81E-02	4732~451a	chr17
hsa-miR-650	9.01	7.92E-03		
hsa-miR-488-3p	8.57	5.12E-03		
hsa-miR-592	7.99	1.95E-02		
hsa-miR-223-3p	7.72	2.73E-04		
hsa-miR-193a-3p	7.32	4.56E-02		
hsa-miR-942-5p	7.29	2.36E-02		
hsa-miR-886-5p	5.99	3.41E-02		
hsa-miR-146b-5p	5.51	9.65E-03		
hsa-miR-720	5.35	1.18E-02		
hsa-miR-27a-3p	5.26	7.91E-05	23a~24-2	chr19
hsa-miR-638	5.19	1.55E-02		
hsa-miR-335-3p	5.01	2.67E-02		
hsa-miR-146a-5p	4.80	8.42E-03		
hsa-miR-140-5p	4.65	1.09E-02		
hsa-miR-199b-3p	4.54	3.08E-02	3154~199b	chr9
hsa-miR-886-3p	4.51	2.07E-02		
hsa-miR-301a-3p	4.51	1.08E-02		

hsa-miR-1274A	4.42	1.60E-02		
hsa-miR-30d-3p	4.35	3.95E-02	30b~30d	chr8
hsa-miR-222-3p	4.28	4.31E-02	222-221	chrX
hsa-miR-16-5p	3.84	4.01E-03		
hsa-miR-374a-5p	3.75	3.27E-02	374a~545	chrX
hsa-miR-126-5p	3.27	2.57E-02		
hsa-miR-106b-5p	3.27	7.43E-03	106b~25	chr7
hsa-miR-34a-5p	3.14	1.71E-02		
hsa-miR-106a-5p	3.13	1.55E-03	106a~363	chrX
hsa-miR-20b-5p	3.07	9.59E-03	106a~363	chrX
hsa-miR-17-5p	3.00	1.89E-03	17~92a-1	chr13
hsa-miR-28-5p	2.95	9.09E-03		
hsa-miR-9-5p	2.89	4.81E-02		
hsa-miR-100-5p	2.80	0.023391658	100~let7a-2	chr11
hsa-miR-152-3p	2.56	0.047124119		
hsa-miR-20a-5p	2.44	2.45E-02	17~92a-1	chr13

Table 12. MicroRNAs displaying significantly downregulated expression in infratentorial pLGGs with respect to normal cerebellum (CTRL). Abbreviations: LFC, Linear Fold Change; Chr, Chromosome

microRNA	**LFC**	**P-value**	**Part of cluster**	**Chr**
hsa-miR-129-2-3p	0.001	1.55E-04		
hsa-miR-302a-5p	0.002	1.27E-02	302b~367	chr4
hsa-miR-206	0.009	4.93E-03	206~133b	chr6
hsa-miR-124-3p	0.012	1.87E-04		
hsa-miR-488-5p	0.013	5.97E-03		

hsa-miR-522-3p	0.015	1.13E-02	512-1~519a-2	chr19
hsa-miR-383-5p	0.021	1.17E-02		
hsa-miR-1296-5p	0.022	9.70E-04		
hsa-miR-519e-3p	0.024	2.11E-02	512-1~519a-2	chr19
hsa-miR-411-3p	0.032	1.27E-02	379~656	chr14
hsa-miR-874-3p	0.033	1.12E-03		
hsa-miR-326	0.035	3.69E-02		
hsa-miR-642a-5p	0.045	3.62E-02	642a~742b	chr19
hsa-miR-589-5p	0.060	4.42E-02		
hsa-miR-885-5p	0.062	8.37E-05		
hsa-miR-668-3p	0.063	2.64E-02	379~656	chr14
hsa-miR-770-5p	0.065	6.11E-03		
hsa-miR-433-3p	0.066	1.44E-02	493~136	chr14
hsa-miR-204-5p	0.074	8.44E-03		
hsa-miR-1227-3p	0.075	1.09E-02	6789~1227	chr19
hsa-miR-149-5p	0.087	8.73E-05		
hsa-miR-485-3p	0.087	3.12E-02	379~656	chr14
hsa-miR-543	0.090	1.25E-02	379~656	chr14
hsa-miR-29b-2-5p	0.108	0.04487562	29b-2~29c	chr1
hsa-miR-7-1-3p	0.135	4.20E-02		
hsa-miR-487b-3p	0.141	1.06E-03	379~656	chr14
hsa-miR-29c-5p	0.164	2.18E-02	29b-2~29c	chr1
hsa-miR-539-5p	0.169	4.81E-03	379~656	chr14
hsa-miR-99b-3p	0.180	1.37E-02	99b~125a	chr19
hsa-miR-128-3p	0.197	1.44E-02		

hsa-miR-127-3p	0.202	1.36E-03	493~136	chr14
hsa-miR-324-5p	0.209	9.31E-04		
hsa-miR-330-3p	0.210	6.91E-04		
hsa-miR-323a-3p	0.210	1.29E-03	379~656	chr14
hsa-miR-532-3p	0.216	1.57E-03	532~502	chrX
hsa-miR-625-5p	0.218	1.84E-02		
hsa-miR-125a-5p	0.222	3.31E-04	99b~125a	chr19
hsa-miR-486-3p	0.222	3.27E-02		
hsa-miR-320b	0.225	2.43E-02		
hsa-miR-484	0.225	2.82E-03		
hsa-miR-491-5p	0.238	4.30E-04		
hsa-miR-370-3p	0.241	1.73E-02		
hsa-miR-361-5p	0.245	1.23E-03		
hsa-miR-134-5p	0.247	4.22E-02	379~656	chr14
hsa-miR-486-5p	0.267	4.14E-02		
hsa-miR-376a-3p	0.277	2.19E-02		
hsa-miR-193a-5p	0.297	3.90E-02		
hsa-miR-422a	0.310	9.63E-03		
hsa-miR-103a-3p	0.316	2.21E-03		
hsa-miR-766-3p	0.328	1.62E-02		
hsa-miR-655-3p	0.330	3.88E-02	379~656	chr14
hsa-miR-95-3p	0.330	4.20E-02		
hsa-miR-181a-5p	0.348	1.43E-02		
hsa-miR-99b-5p	0.385	7.34E-03	99b~125a	chr19
hsa-miR-339-3p	0.430	8.38E-03		

hsa-miR-26a-5p	0.432	2.00E-02		
hsa-miR-345-5p	0.443	9.25E-03		

Among dysregulated microRNAs, miR-139-5p was noteworthy since it was significantly down-regulated only in supratentorial pLGGs (Table 10) and its downregulated expression has been documented in high-grade gliomas (adult and pediatric) (Dai S. et al., 2015; Yue S. et al., 2015; Miele E. et al., 2013), but still unexplored in pLGGs. Interestingly, the number of differentially expressed microRNAs in pLGGs and pHGGs was lower than that observed when pLGGs were compared with non-neoplastic brain tissues (Tables 13 and 14).

Table 13. MicroRNAs expressed at significantly higher levels in pLGG tissues than in pHGG. Abbreviations: LFC, Linear Fold Change; Chr, Chromosome

microRNA	**LFC vs. pHGG**	**P-value**	**Part of cluster**	**Chr**
hsa-miR-875-5p	42.272	1.17E-02	875~599	8
hsa-miR-378	22.129	9.49E-05		
hsa-miR-22-5p	18.397	5.23E-04		
hsa-miR-7-1-3p	3.815	1.01E-02		
hsa-miR-769-5p	3.334	1.20E-03		
hsa-miR-409-3p	1.853	3.87E-02	379~656	14
hsa-miR-30a-3p	1.755	4.22E-02		
hsa-miR-30e-3p	1.748	2.06E-02	30e~30c-1	1
hsa-miR-625-3p	1.732	4.81E-02		
hsa-miR-126-5p	1.608	1.30E-02		

Table 14. MicroRNAs expressed at significantly lower levels in pLGG tissues than in pHGG. Abbreviations: LFC, Linear Fold Change; Chr, Chromosome

microRNA	LFC vs. pHGG	P-value	Part of cluster	Chr
hsa-miR-29c-5p	0.449	3.44E-02	29b-2~29c	1
hsa-miR-720	0.355	6.30E-04		
hsa-miR-181c-3p	0.346	1.07E-02		
hsa-miR-1227-3p	0.308	3.95E-03		
hsa-miR-1275	0.287	1.79E-03		
hsa-miR-744-3p	0.226	1.39E-02		
hsa-miR-20a-3p	0.220	3.10E-03	17~92a-1	13
hsa-miR-424-3p	0.215	2.16E-02	424~450b	X
hsa-miR-638	0.214	1.39E-04		
hsa-miR-939-5p	0.208	7.91E-07	6849~939	8
hsa-miR-1290	0.207	6.79E-04		
hsa-miR-661	0.206	1.10E-04		
hsa-let-7g-3p	0.204	1.24E-02		
hsa-miR-656-3p	0.203	3.83E-02	379~656	14
hsa-miR-144-3p	0.196	3.17E-02	4732~451a	17
hsa-miR-27b-5p	0.195	6.34E-03	23b~24-1	9
hsa-miR-571	0.172	1.12E-03		
hsa-miR-1291	0.171	1.38E-02		
hsa-miR-941	0.169	1.41E-03	941-1~941-5	20
hsa-miR-21-3p	0.155	6.27E-03		
hsa-miR-1183	0.155	2.26E-02		
hsa-miR-361-3p	0.155	5.69E-05		

hsa-miR-650	0.152	1.37E-05		
hsa-miR-488-5p	0.151	7.39E-03		
hsa-miR-214-5p	0.145	2.98E-03	199a-2~214	1
hsa-miR-596	0.144	2.16E-03		
hsa-miR-1208	0.144	1.75E-06		
hsa-miR-33a-5p	0.143	5.58E-04		
hsa-miR-380-5p	0.124	4.62E-03	379~656	14
hsa-miR-892b	0.121	4.61E-02	891b~892c	X
hsa-miR-663b	0.105	1.30E-02		
hsa-miR-1262	0.104	3.70E-03		
hsa-miR-193b-5p	0.103	1.37E-03	193b~365a	16
hsa-miR-1201	0.100	1.11E-03		
hsa-miR-566	0.100	7.16E-03		
hsa-miR-1303	0.099	1.70E-03		
hsa-miR-338-5p	0.093	4.31E-03	1250~657	17
hsa-miR-376a-5p	0.091	1.19E-02	379~656	14
hsa-miR-1300	0.084	4.81E-04		
hsa-miR-1255b-5p	0.082	7.56E-04		
hsa-miR-1238-3p	0.072	1.37E-02		
hsa-miR-1285-3p	0.070	6.13E-04		
hsa-miR-639	0.061	3.78E-03		
hsa-miR-149-3p	0.052	3.61E-07		
hsa-miR-1825	0.046	1.15E-09		
hsa-miR-1253	0.043	3.65E-07		
hsa-miR-659-3p	0.031	3.03E-09	659~658	22
hsa-miR-1228-5p	0.026	9.98E-04		

hsa-miR-675-5p	0.023	1.43E-04		
hsa-miR-483-3p	0.013	1.30E-04		

The pLGG and pHGG samples segregated into two main clusters, Figure 7.

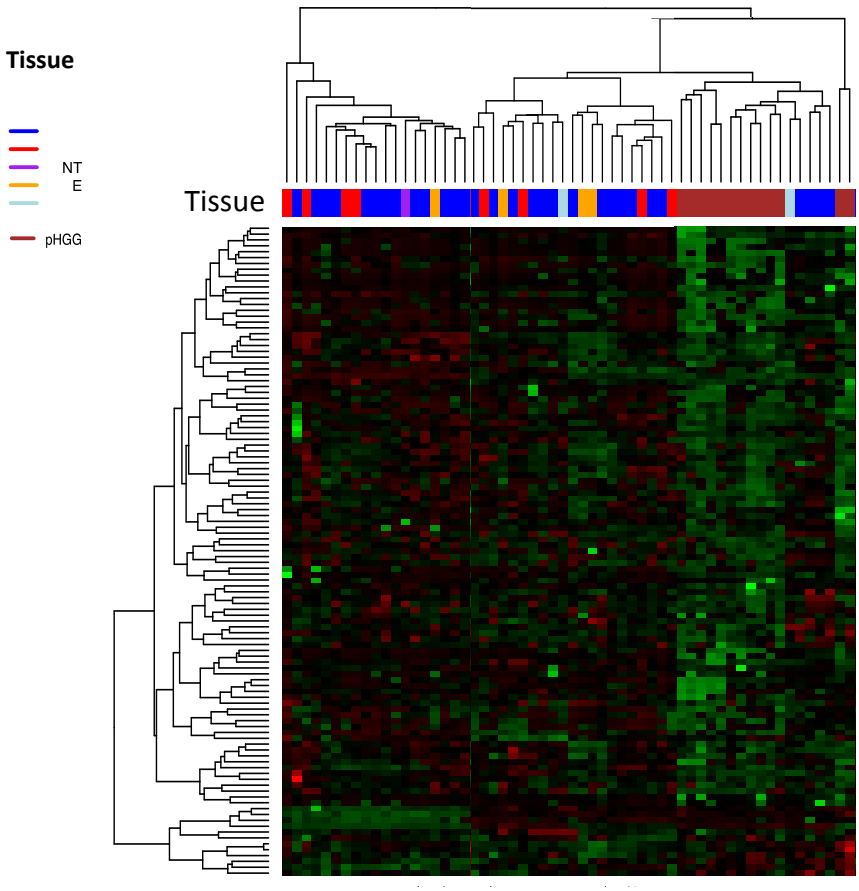

Figure 7. Hierarchical clustering of microRNAs displaying differential expression in pLGGs vs. pHGGs. Hierarchical clustering of the 60 microRNAs differentially expressed in pLGGs vs. pHGGs. The Euclidean method was used to generate clusters based on delta Ct values. Tissue: PA, pilocytic astrocytoma (blue); GG, ganglioglioma (red); GNT, glioneuronal tumour (purple); DNET, disembryoplastic neuroepithelial tumour (orange); AG, angiocentric glioma (light blue); pHGG, pediatric high-grade gliomas (brown).

The first (left side of Figure 7) comprised 19 of the 45 pLGGs. The second (right side of Figure 7) was more heterogeneous and contained two subclusters: one contained 21 pLGGs, the second included both pLGGs and pHGGs. This finding highlighted the existence of a gradient of microRNA expression reflecting internal variation within the pLGGs cohort. Notably, the expression levels of miR-139-5p in pLGGs resembled those found in pHGGs.

5.3 PI3K/AKT signaling is enriched in pLGG

To explore the functional implications of the microRNA profile of our pLGGs cohort, we used the DIANA miRPath tool to identify signaling pathways likely to be vulnerable to the altered microRNA expression levels found in these tumours. As summarized in Table 15**,** after the broader category *pathways in cancer*, the *PI3K/AKT pathway* contained the highest number of components putatively targeted by the microRNAs dysregulated in our pLGG cohort.

Table 15. Enriched biological processes using up- or down- regulated microRNAs in pLGGs. Processes were identified and ranked according to p-value, as assigned in KEGG pathway analysis using DIANA-miRPath (v. 3.0).

	KEGG pathway	p-value	#genes	#microRNAs
Up regulated microRNAs in pLGG vs CTRLs	PI3K-Akt signaling pathway	4.91E-04	223	66
	Signaling pathways regulating pluripotency of stem cells	1.19E-07	104	65
	Focal adhesion	4.91E-04	141	64
	Pathways in cancer	8.43E-06	263	63
	Rap1 signaling pathway	1.50E-04	144	63
	MAPK signaling pathway	9.55E-03	163	62
	Proteoglycans in cancer	3.31E-10	144	62
	Ras signaling pathway	3.51E-04	151	62
	Regulation of actin cytoskeleton	3.10E-03	142	62
	Wnt signaling pathway	1.68E-05	100	61
	Pathways in cancer	5.31E-08	278	58

Down regulated microRNAs in pLGG vs CTRLs	HTLV-I infection	3.07E-02	167	55
	Proteoglycans in cancer	1.82E-07	142	55
	Proteoglycans in cancer	1.82E-07	142	55
	Ras signaling pathway	1.68E-02	146	54
	Regulation of actin cytoskeleton	1.97E-02	141	54
	Axon guidance	1.77E-07	100	53
	Hippo signaling pathway	3.78E-09	114	53
	Oxytocin signaling pathway	1.98E-03	109	53
	PI3K-Akt signaling pathway	6.29E-04	226	53
	Rap1 signaling pathway	6.52E-05	148	53

This finding is consistent with recent reports of aberrant PI3K/AKT/mTOR signaling in pediatric gliomas, both high- and low-grade (Mueller S. et al., 2012; Hütt-Cabezas M. et al., 2013). This hyperactivation has been attributed to genetic and epigenetic alterations in certain glioma subsets, but in many cases the cause is still unknown. We noted with interest, therefore, that *PIK3CA,* which encodes the catalytic subunit of phosphatidylinositol 3–kinase (PI3K), is a validated target of miR-139-5p, as described in Krishnan *et al.* (Krishnan K. et al., 2013). The marked dysregulation of this tumour-suppressor microRNA in pLGGs was documented for the first time in our cohort (Table 8 and Table 10).

5.4 Patients derived pLGG cells and characterization

Taken together, these findings suggested that downregulation of miR-139-5p in supratentorial tumours might contribute to the development of pLGGs by de-repressing expression of PIK3CA, the catalytic subunit of PI3K (Krishnan K. et al., 2013), thereby favoring aberrant activation of the PI3K/AKT pathway. To address this hypothesis, we carried out in vitro experiments in primary monolayer cultures of pLGG cells isolated

from patient-derived samples of AG, DNET, and GG, which are predominantly supratentorial. The characteristics of these cells are summarized in Table 6 and reported in greater detail in Figure 8 and Figure 9.

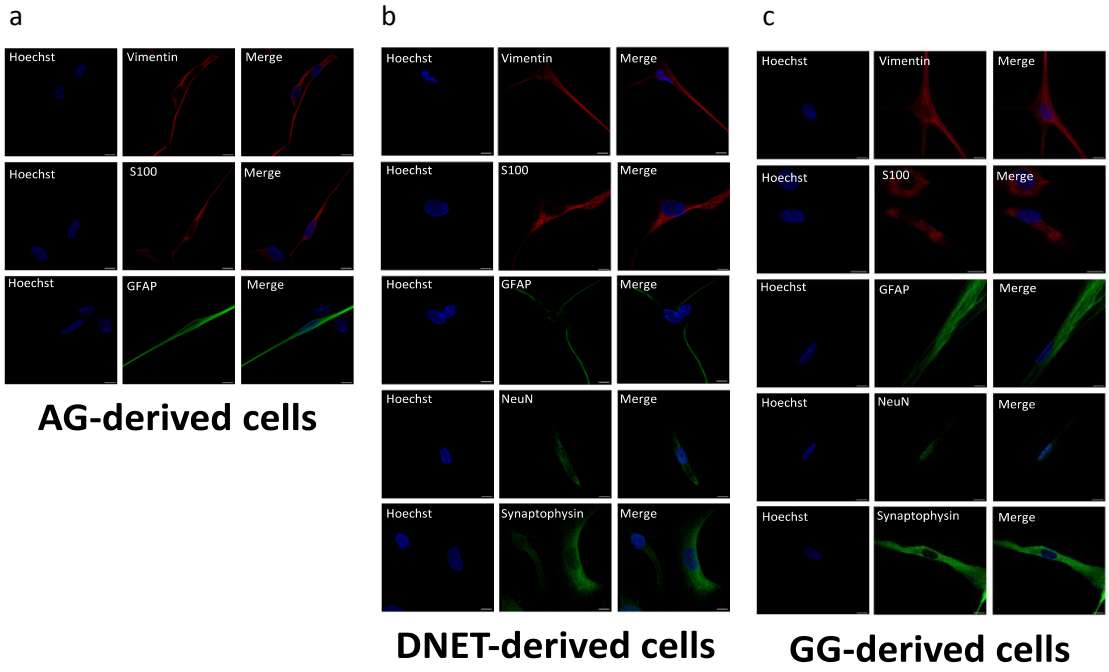

Figure 8. Immunofluorescence characterization of primary patient-derived pLGG cells. (a–c) Single-cell monolayers (on the average present after 7 days of culture) were subjected to immunofluorescence staining for glial markers (S100, vimentin, glial fibrillary acidic protein) and neuronal markers (NeuN, synaptophysin). In detail, (a) AG-derived cells (pLGG1) show positivity for glial markers only (Louis D.N. et al., 2007) whereas (b) DNET-derived cells (findings shown for pLGG2 are also representative of DNET line pLGG3) (Suh Y-L. et al., 2015) and (c) GG-derived cells (pLGG4) expressed both glial and neuronal markers (Luyken C. et al., 2004). The positivity and negativity of the staining of the observed glial and neuronal markers was concordant with immunohistochemical staining results obtained by pathologists on formalin-fixed paraffin-embedded samples of the tumours from which pLGG lines 1, 2, 3 and 4 were derived. Scale bars, 50 and 100 μm (high magnification insert). AG, angiocentric glioma; PLGG, pediatric low-grade gliomas; GG, gangliogliom; DNET, dysembryoplastic neuroepithelial tumour.

The immunofluorescence staining confirmed the glial and/or mixed neuro-glial nature of the primary pLGG cells. For all the histological types, cells were positive for the glial markers vimentin and S100, while the level of glial fibrillary acidic protein positivity was more variable ranging from 20% to 70%. In DNET and GG samples, we also detected frequent positivity for NeuN and Synaptophysin, neuronal markers, which conversely were absent in the AG.

Furthermore, the methylation profiling, a method to evaluate the similarity among tumours samples and their derived primary cells (Selt F. et al., 2017; Sturm D. et al., 2016; Hayes J. et al., 2014; Bracken CP. et al., 2016; Braoudaki M. et al., 2016) indicated that cells are a suitable and trustworthy model to study supratentorial pLGGs biology.

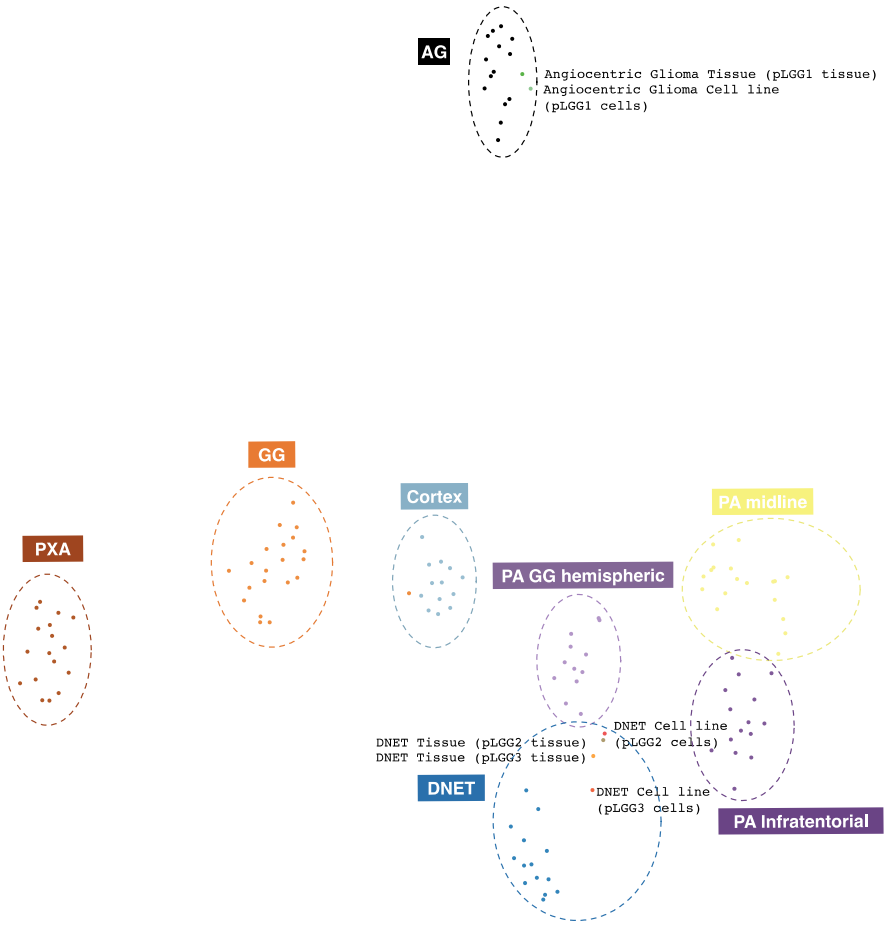

Figure 9. Methylation analysis of primary patient-derived pLGG cells confirms their identity. DNA methylation profiling was performed on the three tumours (an AG and two DNETs) that did not show any genetic BRAF alterations and their primary pLGG derived cells. TSNE (t-distributed stochastic neighbor embedding) analysis of the whole genome DNA methylation data show a close similarity between patient-derived pLGG cell lines, their primary tissues and the group of pLGGs they derive from (AG and DNET) but they diverge from other pediatric low-grade tumours and non-neoplastic cortex. pLGG1, AG tissue and patient-derived cells; pLGG2 and pLGG3, DNET tissues and their respective patient-derived cells (see Table 6). Colour legend of the TSNE plot as follows: PXA (brown); GG (orange); Cortex (light blue); AG (black); PA GG hemispheric (light purple); PA Infratentorial (purple); DNET (blue); PA midline (yellow). PLGG, pediatric low-grade gliomas; AG, angiocentric glioma; DNET, dysembryoplastic neuroepithelial tumour; GG, ganglioglioma; PA, pilocytic astrocytoma; PXA, pleomorphic xanthoastrocytoma.

As previous attempts to use short-term primary cultures of patient-derived pLGGs have been hampered by markedly reduced growth secondary to OIS (Jacob K. et al., 2011;

Raabe E.H. et al., 2011; Selt F. et al., 2017), we have also carefully monitored the rate of senescence over time in our non-PA cultures, Figure 10.

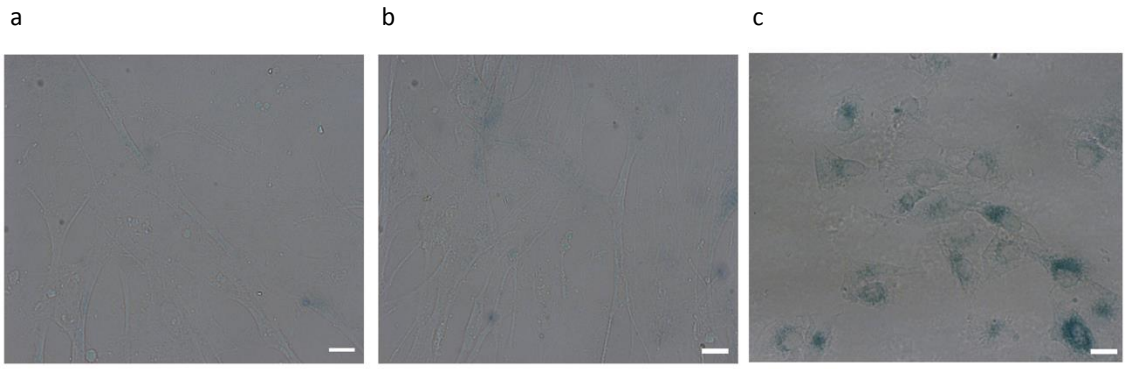

Figure 10. Expression of the senescence marker SA-β-gal in patient-derived primary pLGG cells. Representative images of SA-β-gal expression in two of the primary cell cultures used in the study: (a) pLGG4 cells derived from a GG and (b) pLGG2 cells from a DNET. Both displayed low SA-β-gal-positivity rates (less than 20%) and doubling times that averaged of 72h. In contrast, in panel c a representative image of pLGG4 at passage 12 is reported. The very low proliferation rate and high percentage of SA-β-gal-positive cells reached by these cells rendered them unsuitable for further biological investigations. Scale bar, 100 µm. PLGG, pediatric low-grade gliomas; GG, gangliogliom; DNET, dysembryoplastic neuroepithelial tumour.

Senescence rates varied widely, even between cultures of cells representing the same pLGG histotype, and they generally—but not always—increased over time. For instance, in some cultures, high rates were already observed after the first few passages. By continuously monitoring their senescence rates over time, we were able to complete short-term experiments and our assessment of these cells indicates that they can be used as cellular models of pLGGs.

5.5 Low levels of miR-139-5p in pLGGs regulate tumour-cell proliferation

MiR-139-5p levels in supratentorial pLGGs were markedly lower than those in non-neoplastic total brain tissues (Table 10, Figure 11a). Downregulation of miR-139-5p was also evident in our patient-derived primary pLGG cell cultures at levels comparable to those of the primary tumours they derive from (Figure 11b).

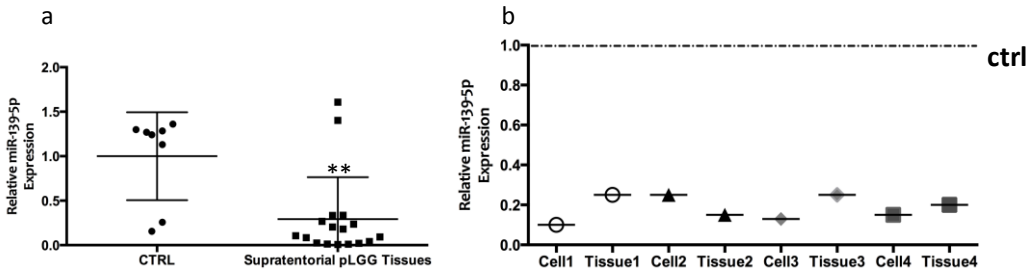

Figure 11. miR-139-5p expression levels in supratentorial pLGG tissues and cells. (a and b) Single assay qPCR validation of downregulated miR-139-5p expression in (a) supratentorial pLGG tissues and (b) patient-derived primary pLGG cell lines and their corresponding tissues vs. non-neoplastic total brain tissue (controls, ctrl). PLGG, pediatric low-grade gliomas.

Overexpression of miR-139-5p in these cells (Figure 12) resulted in significantly reduced proliferation, which was evident in all three histological types represented (Figure 13), while not affecting cell death.

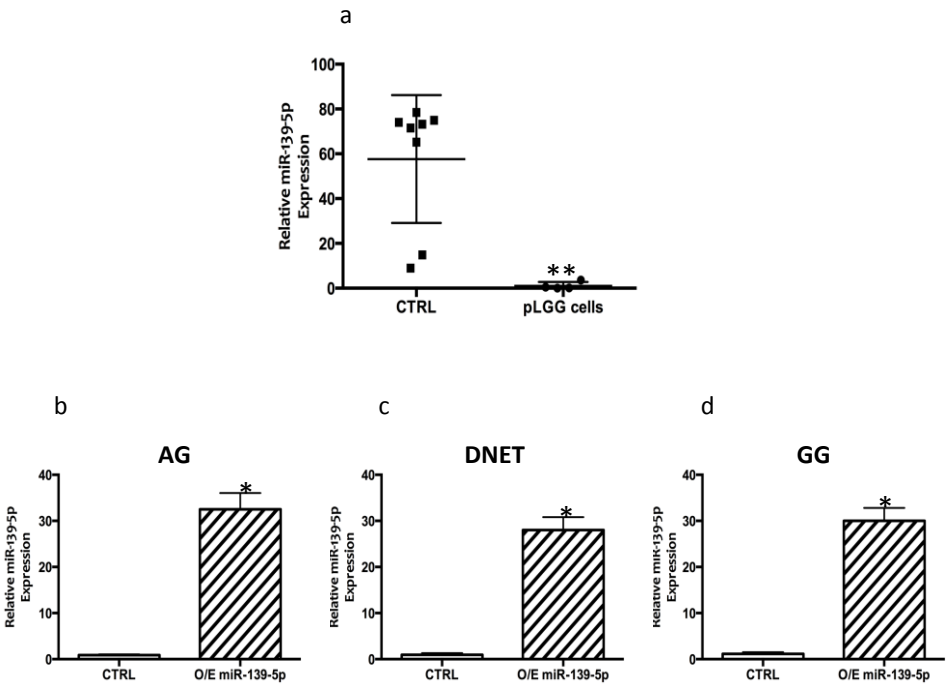

Figure 12. Levels of miR-139-5p before and after its overexpression in the four primary pLGG cell lines (derived from an AG, two DNETs, and a GG). Cells were transfected with 20 nM miR-139-5p and assayed 48 h later. (a) MiR-139-5p level in non-neoplastic brain tissues (CTRL) was 68-fold higher than that found in the pLGG cells at baseline. (b-d) Post-transfection assays of (b) AG cells, (c) DNET cells, and (d) GG cells revealed mean miR-139-5p levels approximately 30-fold higher than those found at baseline (CTRL).

* p<0.05, *** p<0.001 versus indicated CTRL. AG, angiocentric glioma; PLGG, pediatric low-grade gliomas; GG, gangliogliom; DNET, dysembryoplastic neuroepithelial tumour.

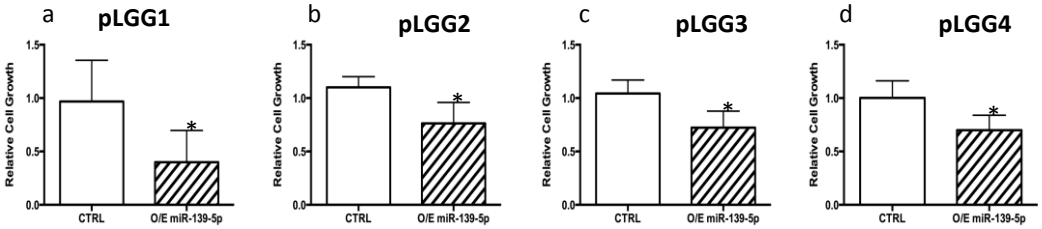

Figure 13. Effects on cell proliferation of miR-139-5p overexpression in cultured cells. Relative cell growth of cultured cells from (a) primary AG, (b) primary DNET indicated as pLGG2, (c) primary DNET indicated as pLGG3 and (d) primary GG. Cells were transfected with 20 nM miR-139-5p or an empty vector (CTRL) and subjected to trypan blue staining 48 h later. Relative cell growth refers to fold over CTRL. * p<0.05 versus CTRL.

5.6 miR-139-5p has a role in the control of PI3K/AKT/mTORC1 signaling in supratentorial pLGGs

The results of the previous experiments provide evidence that downregulation of miR-139-5p plays a role in supratentorial pLGG cell growth. To determine whether its effects on cell growth were mediated by de-repressed PI3K activity, we assessed the effects of miR-139-5p overexpression on the phosphorylation of the PI3K target, AKT. At baseline, phosphorylated AKT (p-AKT) levels were high in all the cell cultures tested, but they dropped markedly after miR-139-5p overexpression, Figure 14.

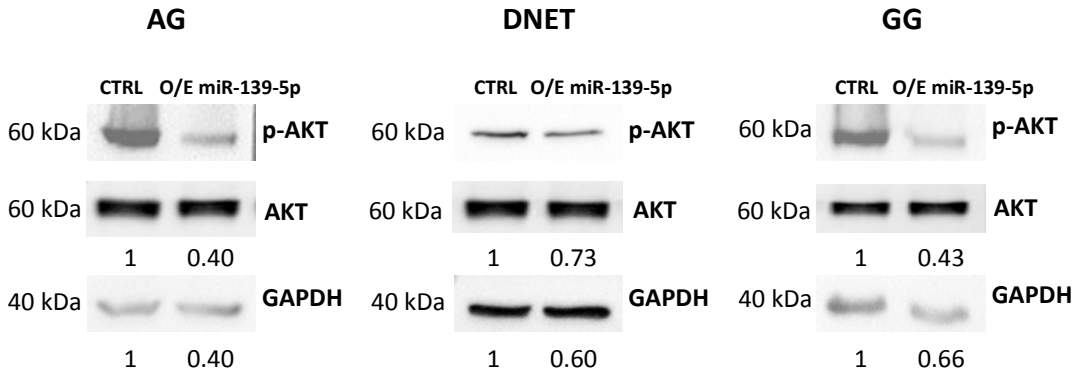

Figure 14. PI3K/AKT signaling pathway inhibition decreases pLGG AKT phosphorylation. Phosphorylated AKT (p-AKT) levels were measured in supratentorial primary pLGG cells transfected with miR-139-5p or empty vector (CTRL). AG, angiocentric glioma; PLGG, pediatric low-grade gliomas; GG, gangliogliom; DNET, dysembryoplastic neuroepithelial tumour.

In order to confirm that miR-139-5p effect was directly mediated by PI3K inhibition, we examined proliferation (Fig. 15a-d) and p-AKT levels (Fig15e-g) in primary pLGG cells before and after treatment with the direct PI3K inhibitor LY294002. Again, we did not observe any significant effect on cell death.

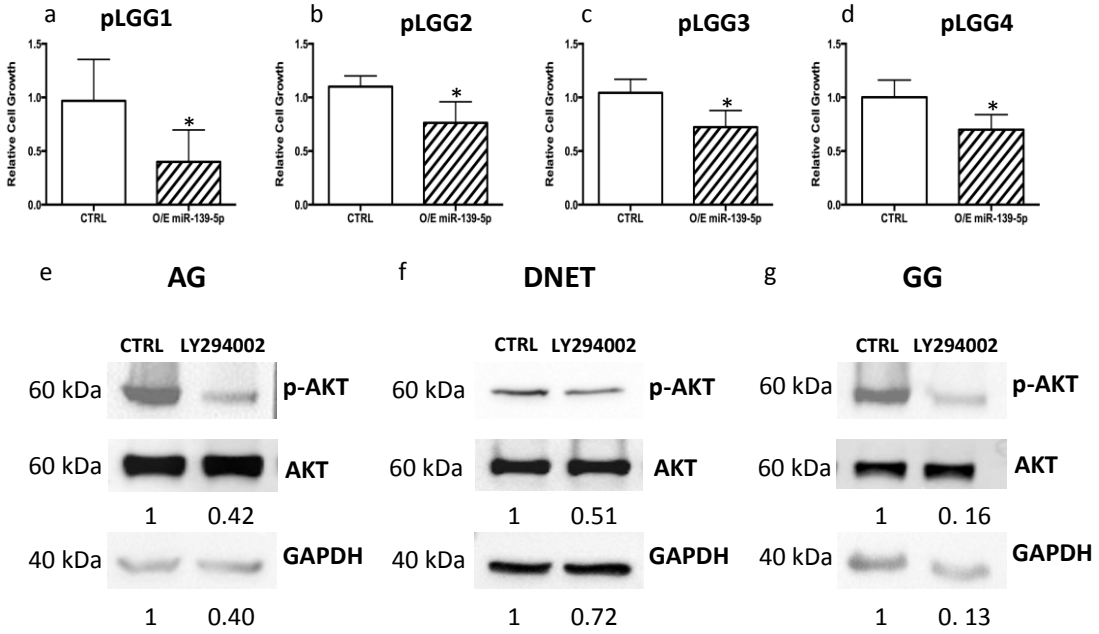

Figure 15. PI3K/AKT signaling pathway inhibition decreases pLGG AKT phosphorylation and cell proliferation. (a-d) pLGG1 (AG), pLGG2 (DNET), pLGG3 (DNET) and pLGG4 (GG) cells were treated for 30 min with 50 μM LY294002 and assayed for proliferation (Trypan blue exclusion) after a 48h recovery period in normal medium. (e–g) p-AKT and total AKT levels were measured in supratentorial primary pLGG cells treated with 50 μM LY294002 for 30 min or vehicle alone (CTRL) after a 48h recovery period in normal medium. Relative cell growth refers to fold over CTRL. *P < 0.05, **P < 0.001 vs. CTRL. AG, angiocentric glioma; PLGG, pediatric low-grade gliomas; GG, gangliogliom; DNET, dysembryoplastic neuroepithelial tumour.

To unravel if the combined effect of miR-139-5p and LY294002 was superimposable to that of miR-139-5p overexpression alone, we overexpressed this microRNA and then treated pLGG2 cells with LY294002. As shown in Figure 16 the combined treatment induced an additional reduction in pLGG cell growth, indicating that miR-139-5p did not act as a single agent in controlling the activation of the PI3K/AKT signaling pathway.

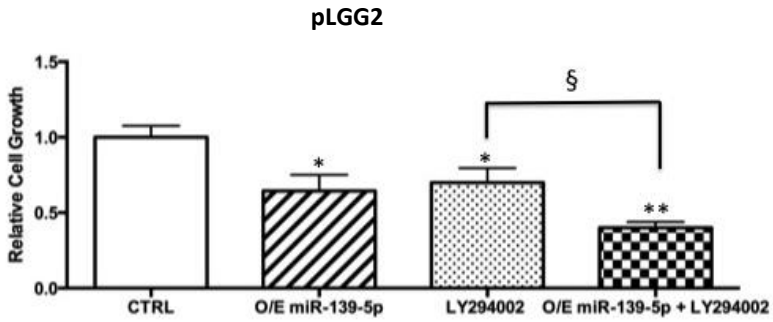

Figure 16. miR-139-5p did not act as a single agent in controlling the activation of the PI3K/AKT signaling pathway. pLGG2 (DNET) cells were transfected with 20 nM miR-139-5p or an empty vector (CTRL) and treated for 30 min with 50 μM LY294002 or vehicle alone (CTRL) and assayed for proliferation (Trypan blue exclusion) after a 48h recovery period in normal medium. Relative cell growth refers to fold over CTRL. *P < 0.05, **P < 0.001 vs. CTRL. PLGG, pediatric low-grade gliomas. DNET, dysembryoplastic neuroepithelial tumour.

One of the downstream effectors of PI3K/AKT signaling is mammalian target of rapamycin complex 1 (mTORC1). Activation of this complex has already been reported in pLGGs (Mueller S. et al., 2012), and hyper-activation of the PI3K/AKT/mTORC1 axis has been implicated in the increased cell proliferation of these tumours (Hütt-Cabezas M. et al., 2013). We therefore wondered if mTORC1 inhibition was involved in the anti-proliferative effects produced in pLGG cells by miR-139-5p overexpression. As shown in Figure 17, cells transfected with miR-139-5p displayed significantly decreased phosphorylation of p70 S6K (p-p70 S6K), a hallmark of mTORC1 activation.

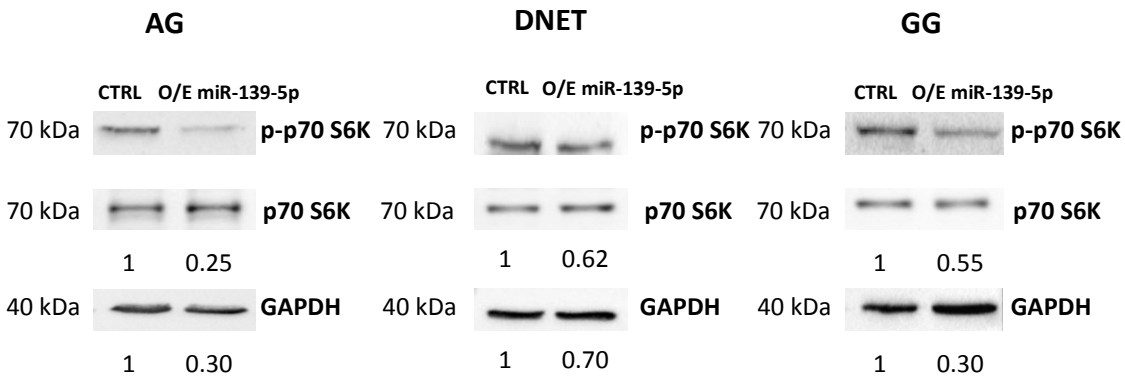

Figure 17. Phosphorylation of p70 S6K in pLGG cells subjected to miR-139-5p overexpression. Phosphorylated p70 S6K (p-p70 S6K) levels were measured in supratentorial primary pLGG cells transfected with miR-139-5p or empty vector (CTRL). AG, angiocentric glioma; PLGG, pediatric low-grade gliomas; GG, gangliogliom; DNET, dysembryoplastic neuroepithelial tumour.

A comparable reduction was produced when PI3K was inhibited with LY294002, Figure 18.

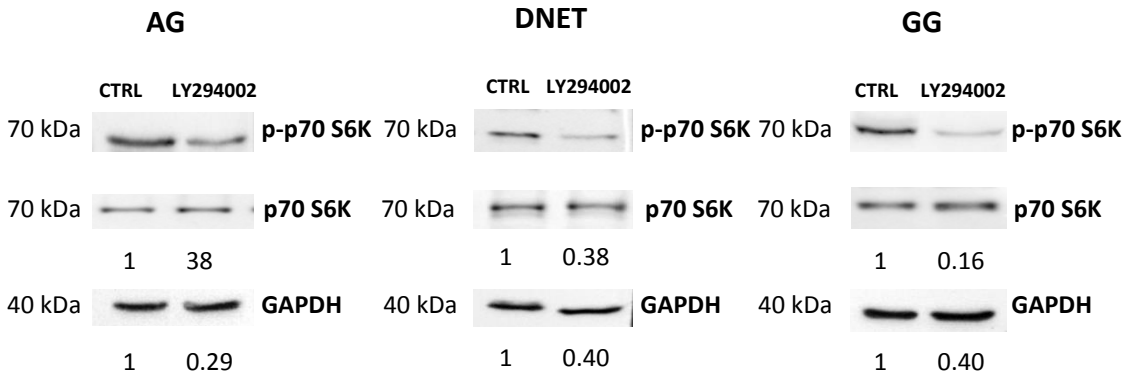

Figure 18. Phosphorylation of p70 S6K in pLGG cells subjected to LY294002 treatment. The direct PI3K inhibition for 30 min with 50 µM LY294002 followed by a 48h recovery period in normal medium both strongly reduced p70 S6K phosphorylated levels (p-p70 S6K). AG, angiocentric glioma; PLGG, pediatric low-grade gliomas; GG, gangliogliom; DNET, dysembryoplastic neuroepithelial tumour.

These data indicate that the downregulated expression of miR-139-5p in primary supratentorial pLGG cells increases their proliferation by de-repressing PI3K/AKT signaling and that its effect is mediated by mTORC1, as summarized in Figure 19.

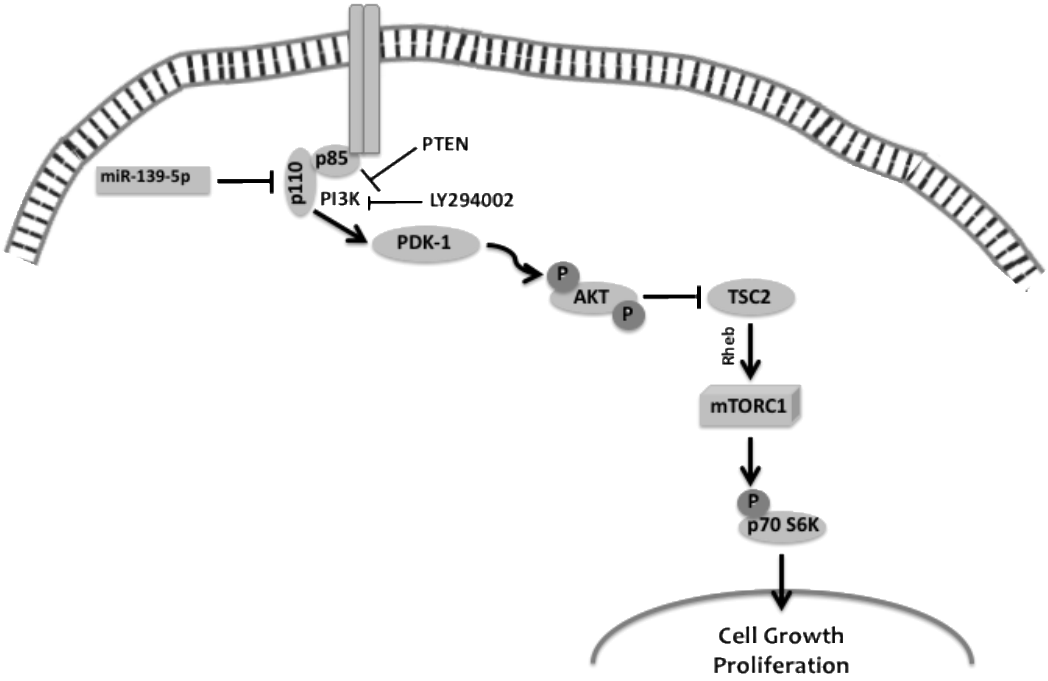

Figure 19. Downregulation of miR-139-5p expression in pLGGs promotes proliferation by de-repressing PI3K/AKT/mTORC1 signaling. miR-139-5p, that targets the 3'-UTR of *PIK3CA*, is strongly downregulated in pLGG tumours resulting in the hyper-activation of the PI3K/AKT pathway. After miR-139-5p overexpression in pLGG primary cells both AKT and p70 S6K phosphorylation levels are reduced, with a consistent significant impairment in cell proliferation. PTEN, phosphatase and tensin homolog; PI3K, phosphatydil-inositol-3-kinase; PDK-1, phosphoinositide-dependent kinase 1; TSC2, tuberous sclerosis complex 2; Rheb, Ras homolog enriched in brain; mTORC1, mammalian target of rapamycin 1; p70 S6K, p70 S6 kinase.

6. Discussion

MicroRNAs have been identified as pivotal players in a variety of cancers (Hayes J. et al., 2014; Bracken C.P. et al., 2016). Thus far, however, the research conducted on these noncoding RNA species in pLGGs has been largely descriptive. Moreover, the conclusions that can be drawn from these studies are frequently limited by the small number of cases analysed (Liu F. et al., 2013; Braoudaki M. et al., 2016), the inclusion of high-grade gliomas besides pLGGs (Birks D.K. et al., 2011; Jones T.A. et al., 2015) or the inclusion of adult patients (Ames H.M. et al., 2017). Our study differs from its predecessors in several respects. Our microRNA profiling study was conducted on fresh-frozen samples of 45 pLGGs, all of which were grade I tumours resected from patients 16 years of age or younger. We identified 93 microRNAs whose differential expression distinguished the pLGGs from controls. Since a number of microRNAs display directional and quantitative similar dysregulation in pHGG, these microRNAs are more likely to play a role in pediatric gliomas in general than in specific WHO classes of pLGGs. In fact, the downregulated expression of miR-487b, miR-323a-3p, and miR-410—all members of the 379-656 cluster—has already been described in gliomas of various grades (Ames H.M. et al., 2017; Laddha S.V. et al., 2013; Skalsky R.L. et al., 2011). Likewise, upregulated expression of miR-18a-5p and miR-20a-5p (both belonging to the miR 17-92 cluster) and of miR-21-5p has been found in pLGGs (Ames H.M. et al., 2017) and pHGGs (Miele E. et al., 2013; Jha P. et al., 2015; Yeh W-L. et al., 2015) as well as in other types of brain tumours (Northcott P.A. et al., 2009; Murphy B.L. et al., 2013; Grunder E. et al., 2011). Thanks to the results of this first part of the study we were able to identify specific microRNA profiles for pLGGs that will be object of future experimental investigations. The importance of the PI3K/AKT/mTOR pathway that emerged from our miR pathway analysis was not surprising. Along with the MAPK/ERK axis, it is one of the pathways most frequently upregulated in cancers, including pLGGs (Pfister S. et al., 2009; Zhang J. et al., 2013; Baker S.J. et al., 2016; Khatua S. et al., 2015). Aberrant activation of PI3K/AKT/mTOR signaling in pLGGs has been linked to several genetic alterations, including *BRAF* fusions, *FGFR1* duplications, and *MYB* rearrangements (Zhang J. et al., 2013), which are present at different frequencies in the various pLGGs histologies, with the last two genetic alterations that have been more specifically detected in DNET and AG, respectively. Epigenetic mechanisms have been investigated as alternative

activators of PI3K signaling in these tumours. For instance, promoter methylation and consequent silencing of expression of the gene encoding PTEN—a major negative regulator of PI3K signaling—has also been documented in some gliomas, and its frequency correlated positively with tumour grading (Mueller S. et al., 2012; Wiencke J.K. et al., 2007). Therefore, *PTEN* promoter methylation, too, is unlikely to account for the oncogenic activation of the PI3K/AKT signaling in most grade I pLGGs. These considerations heightened our interest in the marked downregulation of miR-139-5p, which was found in all examined grade I pLGGs. This microRNA is a known negative regulator of the *PIK3CA* gene, which encodes the catalytic subunit of the PI3K (Krishnan K. et al., 2013). The oncosuppressive effects of miR-139-5p have been described in a variety of solid tumours (Qiu G. et al., 2015; Krishnan K. et al., 2013; Zhang L. et al., 2014; Song M. et al., 2014; Li R.Y. et al., 2013), including adult and pediatric high-grade gliomas (Dai S. et al., 2015; Yue S. et al., 2015; Miele E. et al., 2013). Nonetheless, the expression of miR-139-5p has never been explicitly investigated in pLGGs. Our functional characterization of miR-139-5p loss in grade I pLGGs provides the first evidence that this alteration may be a key driver of oncogenic activation of the PI3K/AKT/mTORC1 pathway in these tumours. As illustrated in Figure 19, the downregulated miR-139-5p expression in supratentorial pLGGs significantly enhances activation of PI3K/AKT/mTORC1 signaling, as reflected by the high phosphorylation levels of AKT and p70 S6K, which dropped markedly after miR-139-5p overexpression, and the biological outcome is a substantial increase in tumour-cell proliferation. As suggested by the experiment reported in Figure 16, miR-139-5p downregulation did not act alone to activate this pathway therefore we cannot exclude additional molecular mechanisms in which miR-139-5p is involved in these tumours. Conversely, its downregulation seems to be complementary to the presence of the genetic and/or epigenetic mechanisms of activation discussed above. It is also important to recall that miR-139-5p downregulation might produce additional tumour-promoting effects by depressing other targets, which include numerous genes with documented oncogenic effects in gliomas and in other cancers as well (e.g., FOS, HRAS, JUN, MCL1, NOTCH1, ELTD1, ZEB1 and ZEB2) (Dai S. et al., 2015; Yue S. et al., 2015; Krishnan K. et al., 2013; Baker S.J. et al., 2016; Wiencke J.K. et al., 2007; Zhang L. et al., 2014; Song M. et al., 2014). These conclusions are based on the results of studies on the restored expression of miR-139-5p in primary cultures of

patient-derived supratentorial pLGG cells, whereas the few functional studies that have been conducted in this area have utilized immortalized pLGG cells, such as the PA-derived Res186 line and/or Res259 cells, which were originally derived from a grade II diffuse astrocytoma (Hütt-Cabezas M. et al., 2013; Li R.Y. et al., 2013; Fan Q. et al., , 2013; H-d Z. et al., 2015). A major drawback of these cell lines is that they harbor genetic alterations that are relatively rare in pLGGs, and it is unclear to what extent they represent the primary lesions (Hütt-Cabezas M. et al., 2013; Brandt W.D. et al., 2015; Ajeawung N.F. et al., 2013). Previous attempts to use short-term primary cultures of patient-derived pLGGs have been hampered by the reduced cell proliferation rate and the onset of the oncogene induced senescence (Jacob K. et al., 2011; Raabe E.H. et al., 2011; Selt F. et al., 2017). Protocol differences might contribute to explain why our efforts were more successful. It is worth noting, however, that the unsuccessful attempts cited above all involved the use of cells isolated from PAs, whereas the cells we used came from non-PA pLGGs. This choice was based on our purpose to elucidate the biology of pLGGs arising in supratentorial structures of the brain, where PAs are less common. Interestingly, however, we also encountered slow growth and senescence in our non-PA cultures. By carefully selecting the cultures destined for experiments particularly by analysing their whole genome methylation profile as method to evaluate the similarity among tumours samples and their derived primary cells (Selt F. et al., 2017; Sturm D. et al., 2016; Lambert S.R. et al., 2013; Hovestadt V. et al., 2013; Sturm D. et al., 2012) but also continuously monitoring their senescence rates over time, we were able to complete short-term experiments and our assessment of these cells indicates that they are likely to provide reliable representations of the pLGGs seen in the clinic. Therefore, our primary patient-derived pLGG cells present many benefits in comparison with the few immortalized cell lines that have been used until now and represent a more reliable model to study the biology of these tumours, that otherwise would be hardly addressed. The major disadvantage of these cultures is that they represent short-term cultures with a low proliferation rate and the number of experiments that can be performed is limited. Consequently, these primary models can be used only to answer to specific and well-defined biological questions. Notably, the methylation profiling allowed us to note that short-term primary cells could be more or less, closer to their primary tumour, probably reflecting the heterogeneity of the cellular composition of the

primary pLGG tumours analysed. Since morbidity and mortality, particularly due to disease progression, represent a significant problem in children affected by pLGGs even after many years from diagnosis (Garcia M.A. et al., 2016; Sturm D. et al., 2017; Upadhyaya S.A. et al., 2017) there is an urgent need for the identification and use of less toxic therapies, such as molecular targeted agents, in children with LGGs (Upadhyaya S.A. et al., 2017). In this context, our primary patients'-derived cellular models represent a proper and trustable *in-vitro* model to test molecular targeted compounds. In summary, the identification of miR-139-5p as a major regulator of the PI3K/AKT/mTORC1 axis in supratentorial pLGGs and the establishment of patients'-derived cellular models represent an important advancement and will open new perspectives to deepen the current knowledge on pLGGs biology.

Bibliography

Ajeawung NF, Faure R, Jones C, Kamnasaran D. Preclinical evaluation of dipotassium bisperoxo (picolinato) oxovanadate V for the treatment of pediatric low-grade gliomas. Future Oncol 2013; 9: 1215–29

Ames HM, Yuan M, Vizcaìno MA, Yu W, Rodriguez FJ. MicroRNA profiling of low-grade glial and glioneuronal tumours shows an independent role for cluster 14q32. 31 member miR-487b. Mod Pathol 2017; 30: 204–16

Baker SJ, Ellison DW, Gutmann DH. Pediatric gliomas as neurodevelopmental disorders. Glia 2016; 64: 879-95

Bao W, Fu HJ, Xie QS, Wang L, Zhang R, Guo ZY, Zhao J, Meng YL, Ren XL, Wang T. HER2 interacts with CD44 to up-regulate CXCR4 via epigenetic silencing of microRNA-139 in gastric cancer cells. Gastroenterology 2011; 141: 2076–87. e6

Birks DK, Barton VN, Donson AM, Handler MH, Vibhakar R, Foreman NK. Survey of MicroRNA expression in pediatric brain tumours. Pediatric blood & cancer, 2011, 56.2: 211-216.

Bongaarts A, Prabowo AS, Arena A, Anink JJ, Reinten RJ, Jansen FE, Spliet WGM, Thom M, Coras R, Blümcke I, Kotulska K, Jozwiak S, Grajkowska W, Söylemezoğlu F, Pimentel J, Schouten-van Meeteren AYN, Mills JD, Iyer AM, van Vliet EA, Mühlebner A, Aronica E. MicroRNA519d and microRNA4758 can identify gangliogliomas from dysembryoplastic neuroepithelial tumours and astrocytomas. Oncotarget, 2018, 9.46: 28103.

Bracken CP, Scott HS, Goodall GJ. A network-biology perspective of microRNA function and dysfunction in cancer. Nature Reviews Genetics 2016; 17: 719-32

Brandt WD, Schreck KC, Bar EE, Taylor I, Marchionni L, Raabe E, Eberhart CG, Rodriguez FJ. Notch signaling activation in pediatric low-grade astrocytoma. J Neuropathol Exp Neurol 2015; 74: 121–31

Braoudaki M, Lambrou G, Papadodima S, Stefanaki K, Prodromou N, Kanavakis E. MicroRNA expression profiles in pediatric dysembryoplastic neuroepithelial tumours. Medical Oncology 2016; 33: 5

Calin GA, Dumitru CD, Shimizu M, Bichi R, Zupo S, Noch E, Aldler H, Rattan S, Keating M, Rai K, Rassenti L, Kipps T, Negrini M, Bullrich F, Croce CM. Frequent deletions and down-regulation of micro-RNA genes miR15 and miR16 at 13q14 in chronic lymphocytic leukemia. Proceedings of the National Academy of Sciences, 2002, 99.24: 15524-15529.

Chou C-H, Chang N-W, Shrestha S, Hsu S-D, Lin Y-L, Lee W-H, Yang C-D, Hong H-C, Wei T-Y, Tu S-J. miRTarBase 2016: updates to the experimentally validated miRNA-target interactions database. Nucleic Acids Res 2015; 44: D239–47

Dai S, Wang X, Li X, Cao Y. MicroRNA-139-5p acts as a tumour suppressor by targeting ELTD1 and regulating cell cycle in glioblastoma multiforme. Biochem Biophys Res Comm 2015; 467: 204–10

Dancey J. mTOR signaling and drug development in cancer. Nature reviews Clinical oncology, 2010, 7.4: 209.

Debacq-Chainiaux F, Erusalimsky JD, Campisi J, Toussaint O. Protocols to detect senescence-associated beta-galactosidase (SA-βgal) activity, a biomarker of senescent cells in culture and in vivo. Nature protocols 2009; 4: 1798-806

Diniz MG, Gomes CC, Guimarães BVA, Castro WH, Lacerda JCT, Cardoso SV, de Faria PR, Dias FL, Eisenberg ALA, Loyola AM. Assessment of BRAFV600E and SMOF412E mutations in epithelial odontogenic tumours. Tumour Biol 2015; 36: 5649–53

Eguía-Aguilar P, Pérezpeña-Díazconti M, Benadón-Darszon E, Chico-Ponce de León F, Gordillo-Domínguez L, Torres-García S, Sadowinski-Pine S, Arenas-Huertero F. Reductions in the expression of miR-124-3p, miR-128-1, and miR-221-3p in pediatric astrocytomas are related to high-grade supratentorial, and recurrent tumours in Mexican children. Child's Nervous System, 2014, 30.7: 1173-1181.

Fan Q, He M, Deng X, Wu WK, Zhao L, Tang J, Wen G, Sun X, Liu Y. Derepression of c-Fos caused by MicroRNA-139 down-regulation contributes to the metastasis of human hepatocellular carcinoma. Cell biochemistry and function 2013; 31: 319-2

Filbin MG, Sturm D. "Gliomas in children." Seminars in neurology. Thieme Medical Publishers, 2018; Vol. 38. No. 01.

Garcia MA, Solomon DA, Haas-Kogan DA. Exploiting molecular biology for diagnosis and targeted management of pediatric low-grade gliomas. Future Oncology 2016; 12: 1493-506

Griffiths-Jones S, Saini HK, van Dongen S, Enright AJ. miRBase: tools for microRNA genomics. Nucleic Acids Res 2007; 36: D154–8

Grunder E, D'Ambrosio R, Fiaschetti G, Abela L, Arcaro A, Zuzak T, Ohgaki H, Lv S-Q, Shalaby T, Grotzer M. MicroRNA-21 suppression impedes medulloblastoma cell migration. European journal of cancer 2011; 47: 2479-90

Guo H, Hu X, Ge S, Qian G, Zhang J. Regulation of RAP1B by miR-139 suppresses human colorectal carcinoma cell proliferation. Int J Biochem Cell Biol 2012; 44: 1465–72

H-d Z, L-h J, D-w S, Li J, Tang J-H. MiR-139-5p: promising biomarker for cancer. Tumor Biol 2015; 36: 1355–65

Hayes J, Peruzzi PP, Lawler S. MicroRNAs in cancer: biomarkers, functions and therapy. Trends in molecular medicine 2014; 20: 460-9

Ho CY, Bar E, Giannini C, Marchionni L, Karajannis MA, Zagzag D, Gutmann DH, Eberhart CG, Rodriguez FJ. MicroRNA profiling in pediatric pilocytic astrocytoma reveals biologically relevant targets, including PBX3, NFIB, and METAP2. Neuro-oncology, 2012, 15.1: 69-82.

Hovestadt V, Remke M, Kool M, Pietsch T, Northcott PA, Fischer R, Florence M, Cavalli G, Ramaswamy V, Zapatka M. Robust molecular subgrouping and copynumber profiling of medulloblastoma from small amounts of archival tumour material using high-density DNA methylation arrays. Acta Neuropathol 2013; 125: 913

Hütt-Cabezas M, Karajannis MA, Zagzag D, Shah S, Horkayne-Szakaly I, Rushing EJ, Cameron JD, Jain D, Eberhart CG, Raabe EH. Activation of mTORC1/mTORC2 signaling in pediatric low-grade glioma and pilocytic astrocytoma reveals mTOR as a therapeutic target. Neuro-oncology 2013; 15: 1604-14

Iorio MV, Ferracin M, Liu CG, Veronese A, Spizzo R, Sabbioni S, Magri E, Pedriali M, Fabbri M, Campiglio M, Ménard S, Palazzo JP, Rosenberg A, Musiani P, Volinia S, Nenci I, Calin GA, Querzoli P, Negrini M, Croce CM. MicroRNA gene expression deregulation in human breast cancer. Cancer Res, 2005; 65: 7065-7070

Jacob K, Quang-Khuong D-A, Jones DT, Witt H, Lambert S, Albrecht S, Witt O, Vezina C, Shirinian M, Faury D. Genetic aberrations leading to MAPK pathway activation mediate oncogene-induced senescence in sporadic pilocytic astrocytomas. Clinical Cancer Research 2011; 17: 4650-60

Jha P, Agrawal R, Pathak P, Kumar A, Purkait S, Mallik S, Suri V, Chand Sharma M, Gupta D, Suri A. Genome-wide small noncoding RNA profiling of pediatric high-grade gliomas reveals deregulation of several miRNAs, identifies downregulation of snoRNA cluster HBII-52 and delineates H3F3A and TP53 mutant-specific miRNAs and snoRNAs. International journal of cancer 2015; 137: 2343-53

Jones DT, Kocialkowski S, Liu L, Pearson DM, Bäcklund LM, Ichimura K, Collins VP. Tandem duplication producing a novel oncogenic BRAF fusion gene defines the majority of pilocytic astrocytomas. Can Res 2008; 68: 8673–7

Jones DT, Kocialkowski S, Liu L, Pearson DM, Ichimura K, Collins VP. Oncogenic RAF1 rearrangement and a novel BRAF mutation as alternatives to KIAA1549: BRAF fusion in activating the MAPK pathway in pilocytic astrocytoma. Oncogene, 2009, 28.20: 2119.

Jones TA, Jeyapalan JN, Forshew T, Tatevossian RG, Lawson AR, Patel SN, Doctor GT, Mumin MA, Picker SR, Phipps KP. Molecular analysis of pediatric brain tumours identifies microRNAs in pilocytic astrocytomas that target the MAPK and NF-κB pathways. Acta neuropathologica communications 2015; 3: 86

Khatua S, Wang J, Rajaram V. Review of low-grade gliomas in children—evolving molecular era and therapeutic insights. Child's Nervous System 2015; 31: 643-52

Krishnan K, Steptoe AL, Martin HC, Pattabiraman DR, Nones K, Waddell N, Mariasegaram M, Simpson PT, Lakhani SR, Vlassov A. miR-139-5p is a regulator of metastatic pathways in breast cancer. Rna 2013; 19: 1767-80

Laddha SV, Nayak S, Paul D, Reddy R, Sharma C, Jha P, Hariharan M, Agrawal A, Chowdhury S, Sarkar C. Genome-wide analysis reveals downregulation of miR-379/miR-656 cluster in human cancers. Biology direct 2013; 8: 10

Lambert SR, Witt H, Hovestadt V, Zucknick M, Kool M, Pearson DM, Korshunov A, Ryzhova M, Ichimura K, Jabado N. Differential expression and methylation of brain developmental genes define location-specific subsets of pilocytic astrocytoma. Acta Neuropathol 2013; 126: 291–301

Lewis BP, Shih IH, Jones-Rhoades MW, Bartel DP, Burge CB. Prediction of mammalian microRNA targets. Cell, 2003, 115.7: 787-798.

Lin S, Gregory RI. MicroRNA biogenesis pathways in cancer. Nature reviews cancer, 2015, 15.6: 321.

Liu F, Xiong Y, Zhao Y, Tao L, Zhang Z, Zhang H, Liu Y, Feng G, Li B, He L. Identification of aberrant micro-RNA expression pattern in pediatric gliomas by microarray. Diagn Pathol 2013; 8: 158

Louis DN, Ohgaki H, Wiestler OD, Cavenee WK, Burger PC, Jouvet A, Scheithauer BW, Kleihues P. The 2007 WHO classification of tumours of the central nervous system. Acta Neuropathol 2007; 114: 97–109

Louis DN, Perry A, Reifenberger G, Von Deimling A, Figarella-Branger D, Cavenee WK, Ohgaki H, Wiestler OD, Kleihues P, Ellison DW. The 2016 World Health Organization classification of tumours of the central nervous system: a summary. Acta Neuropathol 2016; 131: 803–20

Luyken C, Bl€umcke I, Fimmers R, Urbach H, Wiestler OD, Schramm J. Supratentorial gangliogliomas: histopathologic grading and tumour recurrence in 184 patients with a median follow-up of 8 years. Cancer 2004; 101: 146–55

Mao R, Zou F, Yang L, Lin S, Li Y, Ma M, Yin P, Liang X, Liu J. The loss of MiR-139-5p promotes colitis-associated tumorigenesis by mediating PI3K/AKT/Wnt signaling. Int J Biochem Cell Biol 2015; 69: 153–61

Miele E, Buttarelli FR, Arcella A, Begalli F, Garg N, Silvano M, Po A, Baldi C, Carissimo G, Antonelli M. High-throughput microRNA profiling of pediatric highgrade gliomas. Neuro-Oncology 2013; 16: 228–40

Mueller S, Phillips J, Onar-Thomas A, Romero E, Zheng S, Wiencke JK, McBride SM, Cowdrey C, Prados MD, Weiss WA. PTEN promoter methylation and activation of the PI3K/Akt/mTOR pathway in pediatric gliomas and influence on clinical outcome. NeuroOncology 2012;14: 1146–52

Murphy BL, Obad S, Bihannic L, Ayrault O, Zindy F, Kauppinen S, Roussel MF. Silencing of the miR-17∼ 92 cluster family inhibits medulloblastoma progression. Cancer research 2013; 73: 7068-78

Nicolaides TP, Li H, Solomon DA, Hariono S, Hashizume R, Barkovich K, Baker SJ, Paugh BS, Jones C, Forshew T, Hindley GF, Hodgson JG, Kim JS, Rowitch DH, Weiss WA, Waldman TA, James CD. Targeted therapy for BRAFV600E malignant astrocytoma. Clinical Cancer Research, 2011, 17.24: 7595-7604.

Northcott PA, Fernandez-L A, Hagan JP, Ellison DW, Grajkowska W, Gillespie Y, Grundy R, Van Meter T, Rutka JT, Croce CM. The miR-17/92 polycistron is up-regulated in Sonic Hedgehog–driven medulloblastomas and induced by N-myc in Sonic Hedgehog–treated cerebellar neural precursors. Cancer research 2009; 69: 3249-55

Packer RJ, Pfister S, Bouffet E, Avery R, Bandopadhayay P, Bornhorst M, Bowers DC, Ellison D, Fangusaro J, Foreman N. Pediatric low-grade gliomas: implications of the biologic era. Neuro-oncology 2016; 19: 750-61

Pfister S, Witt O. Pediatric Gliomas. In Gliomas Ed. A von Deimling. Berlin, Heidelberg: Springer Berlin Heidelberg. 2009: 67-81

Po A, Silvano M, Miele E, Capalbo C, Eramo A, Salvat iV, Todaro M, Besharat Z, Catanzaro G, Cucchi D, Coni S, Di Marcotullio L, Canettieri G, Vacca A, Stassi G, De Smaele E, Tartaglia M, Screpanti I, De Maria R, Ferretti E. Noncanonical GLI1 signaling promotes stemness features and in-vivo growth in lung adenocarcinoma Oncogene 2017; 36: 4641–4652

Qaddoumi I, Orisme W, Wen J, Santiago T, Gupta K, Dalton JD, Tang B, Haupfear K, Punchihewa C, Easton J. Genetic alterations in uncommon low-grade neuroepithelial tumours: BRAF, FGFR1, and MYB mutations occur at high frequency and align with morphology. Acta Neuropathol 2016; 131: 833–45

Qiu G, Lin Y, Zhang H, Wu D. miR-139-5p inhibits epithelial–mesenchymal transition, migration and invasion of hepatocellular carcinoma cells by targeting ZEB1 and ZEB2. Biochem Biophys Res Comm 2015; 463: 315–21

Ronci M, Catanzaro G, Pieroni L, Po A, Besharat ZM, Greco V, Levi Mortera S, Screpanti I, Ferretti E, Urbani A. Proteomic analysis of human sonic hedgehog (SHH) medulloblastoma stem-like cells. Mol Biosyst 2015 May 19; 11: 1603-11

Schindler G, Capper D, Meyer J, Janzarik W, Omran H, Herold-Mende C, Schmieder K, Wesseling P, Mawrin C, Hasselblatt M, Louis DN, Korshunov A, Pfister S, Hartmann C, Paulus W, Reifenberger G, von Deimling A. Analysis of BRAF V600E mutation in 1,320 nervous system tumours reveals high mutation frequencies in pleomorphic xanthoastrocytoma, ganglioglioma and extra-cerebellar pilocytic astrocytoma. Acta neuropathologica, 2011, 121.3: 397-405.

Schubbert S, Shannon K, Bollag G. Hyperactive Ras in developmental disorders and cancer. Nat Rev Cancer 2007; 7:295–308.

Selt F, Hohloch J, Hielscher T, Sahm F, Capper D, Korshunov A, Usta D, Brabetz S, Ridinger J, Ecker J. Establishment and application of a novel patient-derived KIAA1549: BRAF-driven pediatric pilocytic astrocytoma model for preclinical drug testing. Oncotarget 2017; 8: 11460

Skalsky RL, Cullen BR. Reduced expression of brain-enriched microRNAs in glioblastomas permits targeted regulation of a cell death gene. PloS one 2011; 6: e24248

Sturm D, Orr BA, Toprak UH, Hovestadt V, Jones DT, Capper D, Sill M, Buchhalter I, Northcott PA, Leis I. New brain tumour entities emerge from molecular classification of CNS-PNETs. Cell 2016; 164: 1060–72

Sturm D, Pfister SM, Jones DT. Pediatric gliomas: Current concepts on diagnosis, biology, and clinical management. Journal of Clinical Oncology 2017: JCO. 2017.73. 0242

Sturm D, Witt H, Hovestadt V, Khuong-Quang DA, Jones DT, Konermann C, Pfaff E, Tönjes M, Sill M, Bender S. Hotspot mutations in H3F3A andIDH1 define distinct epigenetic and biological subgroups of glioblastoma. Cancer Cell 2012; 22: 425– 37

Suh Y-L. Dysembryoplastic neuroepithelial tumours. J Pathol Transl Med 2015; 49: 438

Suh Y-L. Dysembryoplastic neuroepithelial tumours. Journal of pathology and translational medicine 2015; 49: 438

Suzuki R, Shimodaira H. Pvclust: an R package for assessing the uncertainty in hierarchical clustering. Bioinformatics 2006; 22: 1540–2

Tatevossian RG, Lawson AR, Forshew T, Hindley GF, Ellison DW, Sheer D. MAPK pathway activation and the origins of pediatric low-grade astrocytomas. Journal of cellular physiology, 2010, 222.3: 509-514.

Tian Y, Rich BE, Vena N, Craig JM, MacConaill LE, Rajaram V, Goldman S, Taha H, Mahmoud M, Ozek M. Detection of KIAA1549-BRAF fusion transcripts in formalin-fixed paraffin-embedded pediatric low-grade gliomas. J Mol Diagn 2011; 13: 669–77

Upadhyaya SA, Ghazwani Y, Wu S, Broniscer A, Boop FA, Gajjar A, Qaddoumi I. Mortality in children with low-grade glioma or glioneuronal tumours: A single-institution study. Pediatric Blood & Cancer 2017:

Vlachos IS, Zagganas K, Paraskevopoulou MD, Georgakilas G, Karagkouni D, Vergoulis T, Dalamagas T, Hatzigeorgiou AG. DIANA-miRPath v3. 0: deciphering microRNA function with experimental support. Nucleic Acids Res 2015; 43: W460–6

Wiencke JK, Zheng S, Jelluma N, Tihan T, Vandenberg S, Tamg€uney T, Baumber R, Parsons R, Lamborn KR, Berger MS. Methylation of the PTEN promoter defines low-grade gliomas and secondary glioblastoma. Neuro- Oncology 2007; 9: 271–9

Winter J, Jung S, Keller S, Gregory RI, Diederichs S. Many roads to maturity: microRNA biogenesis pathways and their regulation. Nature cell biology, 2009, 11.3: 228.

Wong CCL, Wong CM, Tung EKK, Au SLK, Lee JMF, Poon RTP, Man K, Ng IOL. The microRNA miR-139 suppresses metastasis and progression of hepatocellular carcinoma by down-regulating Rho-kinase 2. Gastroenterology 2011; 140: 322–31

Yeh W-L, Lin H-Y, Huang C-Y, Huang B-R, Lin C, Lu D-Y, Wei K-C. Migration-prone glioma cells show curcumin resistance associated with enhanced expression of miR-21 and invasion/anti-apoptosis-related proteins. Oncotarget 2015; 6: 37770

Yue S, Wang L, Zhang H, Min Y, Lou Y, Sun H, Jiang Y, Zhang W, Liang A, Guo Y. miR-139-5p suppresses cancer cell migration and invasion through targeting ZEB1 and ZEB2 in GBM. Tumour Biol 2015; 36: 6741–9

Zhang J, Wu G, Miller CP, Tatevossian RG, Dalton JD, Tang B, Orisme W, Punchihewa C, Parker M, Qaddoumi I, Boop FA. Project SJCsRHWUPCG. Whole-genome sequencing identifies genetic alterations in pediatric lowgrade gliomas. Nat Genet 2013; 45: 602–12